5 Thermal Infrared Remote Sensing of Water Temperature in Riverine Landscapes

Rebecca N. Handcock[1], Christian E. Torgersen[2], Keith A. Cherkauer[3], Alan R. Gillespie[4], Klement Tockner[5], Russel N. Faux[6] and Jing Tan[3]

[1]Commonwealth Scientific and Industrial Research Organization, Floreat, WA, Australia
[2]U.S. Geological Survey, Forest and Rangeland Ecosystem Science Center, School of Environmental and Forest Sciences, University of Washington, Seattle, WA, USA
[3]Department of Agricultural and Biological Engineering, Purdue University, West Lafayette, IN, USA
[4]Department of Earth and Space Sciences, University of Washington, Seattle, WA, USA
[5]Leibniz-Institute of Freshwater Ecology and Inland Fisheries and Institute of Biology, Freie Universität Berlin, Germany
[6]Watershed Sciences, Inc., Corvallis, OR, USA

5.1 Introduction

Water temperature in riverine landscapes is an important regional indicator of water quality that is influenced by both ground- and surface-water inputs, and indirectly by land use in the surrounding watershed (Brown and Krygier, 1970; Beschta et al., 1987; Chen et al., 1998; Poole and Berman, 2001). Coldwater fishes such as salmon and trout are sensitive to elevated water temperature; therefore, water temperature must meet management guidelines and quality standards, which aim to create a healthy environment for endangered populations (McCullough et al., 2009). For example, in the USA, the Environmental Protection Agency (EPA) has established water quality standards to identify specific temperature criteria to protect coldwater fishes (Environmental Protection Agency, 2003). Trout and salmon can survive in cool-water refugia even when temperatures at other measurement locations are at or above the recommended maximums (Ebersole et al., 2001; Baird and Krueger, 2003; High et al., 2006). Spatially extensive measurements of water temperature are necessary to locate these refugia, to identify the location of ground- and surface-water inputs to the river channel, and to identify thermal pollution sources.

Regional assessment of water temperature in streams and rivers has been limited by sparse sampling in both space and time. Water temperature has typically been measured using a network of widely distributed in-stream gages, which record the temporal change of the

Fluvial Remote Sensing for Science and Management, First Edition. Edited by Patrice E. Carbonneau and Hervé Piégay.

Table 5.1 Comparison of conventional measurements and TIR remote sensing for regional assessment of water temperature in rivers and streams.

a)

		Conventional Measurements	TIR Remote Sensing
Data acquisition	Advantages	• Measurements can be made at any point in the water column. • Limited technical expertise is needed to gather data. • Data can be obtained under most weather conditions including fog and cloud cover. • Continuous measurements are possible using data loggers. • Costs of collecting data can be low, depending on the number of instruments that must be deployed.	• An alternative to collecting validation data is to use existing networks of in-stream data loggers. **Satellite** • Capability for regional coverage, repeat monitoring with systematic image characteristics, and low cost. • Data can be gathered across multiple scales from local (e.g. upwelling ground-water) to regional (entire floodplains). **Airborne** • Can measure TIR images at fine pixel sizes suitable for narrower streams and rivers. **Ground** • Instruments are easy to deploy and validate *in situ*; requires physical access to the stream.
	Disadvantages	• Sparse sampling of T_k in space. • Gives limited information about the spatial distribution of water temperature. Data loggers can be destroyed or removed by vandalism or floods. • Data are collected only at point locations. Do not provide a view the entire thermal landscape of the river. • Temperature gauges are typically located in larger streams and rivers. • Calibration of thermometers is still necessary. • To collect spatially extensive measurements, it is necessary to deploy many personnel.	• Obtaining TIR images can be costly and complex, and temporally limited. • Care must be taken in interpretation of TIR data under off-nadir observation angles and with variable surface roughness (i.e. diffuse versus specular reflections). **Satellite** • TIR images may not be available due to cloud cover, limited duty cycle of platforms used to collect data (satellite orbits, or availability of aircraft). **Airborne** • Generally acquired over narrow swath widths covering small areas compared to satellite data. • Acquisition costs can be high, especially if multiple overlapping scan lines are needed to create a mosaic. **Ground** • Can only view the water from specific locations along the stream. • Observation angles need to be chosen carefully to reduce the effects of reflections from objects along the river bank.

b)

		Conventional Measurements	TIR Remote Sensing
Data Processing	Advantages	• Standard data storage and processing techniques can be used (knowledge of the hydrological system is still necessary).	• For applications in which having a non-absolute temperature is useful, non-radiometrically corrected TIR images can be used to assess relative spatial patterns within a single image. • Validation is not required for applications that only need relative temperatures.
	Disadvantages		• Interpretation of TIR image data to determine water temperature can be complex and expensive, and requires trained technical expertise. • Care must be taken to interpret TIR images within their terrestrial and aquatic context. • Radiometric correction is necessary to accurately retrieve quantitative temperatures from TIR data accurately, but this can be time-consuming and expensive. • For data acquired from aircraft, changes in the stability of the aircraft as it flies can require complex and costly post-processing of images.

Table 5.1 (*continued*).

c)		Conventional Measurements	TIR Remote Sensing
Applications	Advantages	• T_k can be measured directly, which is both of interest biologically and applicable to management objectives.	• Repeatable, spatially extensive, and systematic measurements. • Can quantify spatial patterns of water temperature in streams, rivers, and floodplains at scales ranging from less than 1 m to over 100 km. • Can view the entire thermal landscape of the river, not just point locations. • Consistent data source for entire floodplains and can be used to calibrate stream temperature models. • TIR image data and concurrent visible and NIR images (where available) can be used to assess both the water surface and adjacent riparian areas. • Repeat flights can be used to assess habitat degradation.
	Disadvantages	• Difficult to collect spatially extensive data to use to calibrate stream temperature models for entire watersheds.	• T_r is measured at the surface layer of the water and may not be representative of T_k in the water column, which is of interest biologically. • Trade-off between pixel-size (i.e. to identify spatial patterns and reduce mixing with bank materials) and the cost of conducting broad-scale surveys.

bulk, or kinetic, temperature of the water (T_k) at specific locations. For example, the State of Washington (USA) recorded water quality conditions at 76 stations within the Puget Lowlands eco region, which contains 12,721 km of streams and rivers (Washington Department of Ecology, 1998). Such gages are sparsely distributed, are typically located only in larger streams and rivers, and give limited information about the spatial distribution of water temperature (Cherkauer et al., 2005).

Although hydrologists, ecologists, and resource managers are ultimately interested in T_k in the water column – because this is both biologically important and also the definition of temperature used for management purposes – measurements of radiant temperature (T_r) made at the water's surface using thermal infrared (TIR) remote sensing provide an attractive alternative to *in situ* measurement of T_k, if T_r measurements can be determined with suitable and known quality and detail. A key advantage of TIR remote sensing of T_r over conventional measurements of T_k is that it is possible to quantify spatial patterns of water temperature in rivers, streams, and floodplains, at multiple spatial scales throughout entire watersheds. However, remote sensing of water temperature can be time-consuming and costly due to the difficulties in obtaining images and the complexities of processing raw data to produce calibrated temperature maps. As will be explored in this chapter, understanding these benefits and limitations is necessary to determine whether thermal remote sensing of water temperature is suitable for water resource management applications (Table 5.1).

The goal of this chapter is to show how TIR measurements can be used for monitoring spatial patterns of water temperature in streams and rivers for practical applications in water resources management. We use the term 'water temperature' to refer specifically to water temperature of lotic systems ranging in size from streams to rivers. The chapter is divided into three parts. First, we examine the state of the science and application of TIR remote sensing of streams and rivers Section 5.2. Second, we explore the theoretical basis of TIR measurements of water temperature, data sources suitable for observing riverine landscapes, the required processing steps necessary to obtain accurate estimates of water temperature from TIR data, and the validation of such temperature estimates (Sections 5.3 to 5.6). Third, we show two examples of using TIR data to monitor water temperature in rivers of varying sizes (Sections 5.7 and 5.8). To illustrate the utility of TIR data for quantifying thermal heterogeneity over a range of spatial scales, we show very fine resolution (0.2–1 m) images of fine-scale hydrologic features such as groundwater springs and cold-water seeps. We also expand the scope to entire floodplains and river sections (1–150 km) to show characteristic patterns of lateral and longitudinal thermal variation in riverine landscapes. For TIR pixel sizes, we use the following terminology across a range of sensors and platforms: 'ultra-fine resolution' for pixel sizes of less than 1 m, 'very fine resolution' for pixel sizes of 1 to 5 m, 'fine resolution' for pixel sizes of 5 to 15 m, 'medium resolution' for pixel sizes of 15 to 100 m, and 'coarse resolution' for pixel sizes of greater than 100 m.

5.2 State of the art: TIR remote sensing of streams and rivers

The remote sensing of surface water temperature using measurements of emitted TIR radiation (3–14μm) can provide spatially distributed values of T_r in the 'skin' layer of the water (top 100μm). This is a well-established practice (Mertes et al., 2004), particularly in oceanography where daily observations of regional and global sea-surface temperature (SST) are made from satellites (Anding and Kauth, 1970; Emery and Yu, 1997; Kilpatrick et al., 2001; Parkinson, 2003). In the terrestrial environment, TIR remote sensing of surface water temperature initially focused on lakes (LeDrew and Franklin, 1985; Bolgrien and Brooks, 1992) and coastal applications such as thermal pollution from cooling water discharge from a nuclear power plant (Chen et al., 2003), but starting in the 1990s airborne TIR remote sensing has been conducted by government agencies over thousands of kilometers of rivers to monitor water quality, identify sources of cold-water inputs, and to develop spatially referenced river temperature models (Faux and McIntosh, 2000; Faux et al., 2001; Torgersen et al., 2001).

Applications of TIR technology to measure water temperature of rivers are diverse and have been employed in a wide variety of fluvial environments. Published examples of thermal maps can be found in the early 1970s (Atwell et al., 1971), and one of the earliest documented uses of TIR imaging to evaluate fish habitat in a river was by researchers in Australia, who identified cold groundwater inputs that were ostensibly important for the survival of rainbow trout (*Oncorhynchus mykiss*) in the Murray River (Hick and Carlton, 1991). The TIR images, collected from a fixed-wing aircraft mounted with a multispectral scanner, were particularly effective in the brackish sections of the Murray River where cool groundwater rose to the surface because it was less dense than saltwater. Subsequent work – like that in the Murray River – focused on thermal anomalies associated with wall-based channels, groundwater inputs, and thermal refugia important for salmon in the Pacific Northwest (USA) (Belknap and Naiman, 1998; Torgersen et al., 1999). The impetus for such work arose from the need to identify localised patches of cool water (e.g., Figure 5.1), but the utility of these data became even more apparent for assessing thermal diversity at broader spatial scales in the floodplain (e.g., Figures 5.2, 5.3, and 5.11) and longitudinally over tens of kilometers (Figure 5.4). Direct applications in fisheries continue to be conducted (Madej et al., 2006), but by far the most extensive use of TIR remote sensing has been by natural resource management agencies seeking to calibrate spatially explicit river temperature models for entire watersheds (Figure 5.4; Boyd and Kasper, 2003; Oregon Department of Environmental Quality, 2006). Prior to the availability of near-continuously sampled longitudinal water temperature data derived from airborne TIR remote sensing, discontinuities associated with groundwater inputs and hyporheic flow were very difficult to quantify empirically.

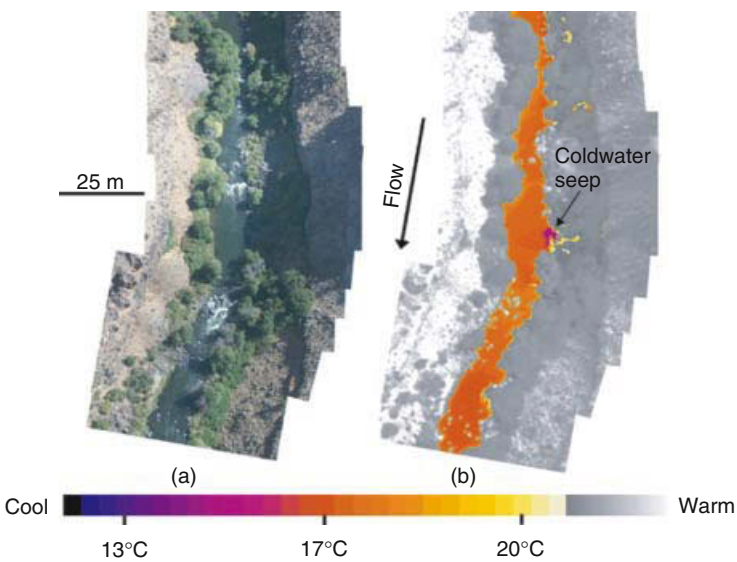

Figure 5.1 Natural-color (a) and airborne TIR (b) aerial images of cold-water seepage area in the Crooked River (Oregon, USA) in a high-desert basalt canyon (27 August 2002). The colored portion of the TIR temperature scale spans the approximate range in water surface temperature in the image; land and vegetation surface temperature are depicted in shades of gray. Lateral cold-water seeps, such as the one depicted above, are relatively small in area but provide important thermal refugia for coldwater fishes. (United States Bureau of Land Management, Dept. of Interior, USA; Watershed Sciences, Inc., Corvallis, Oregon, USA).

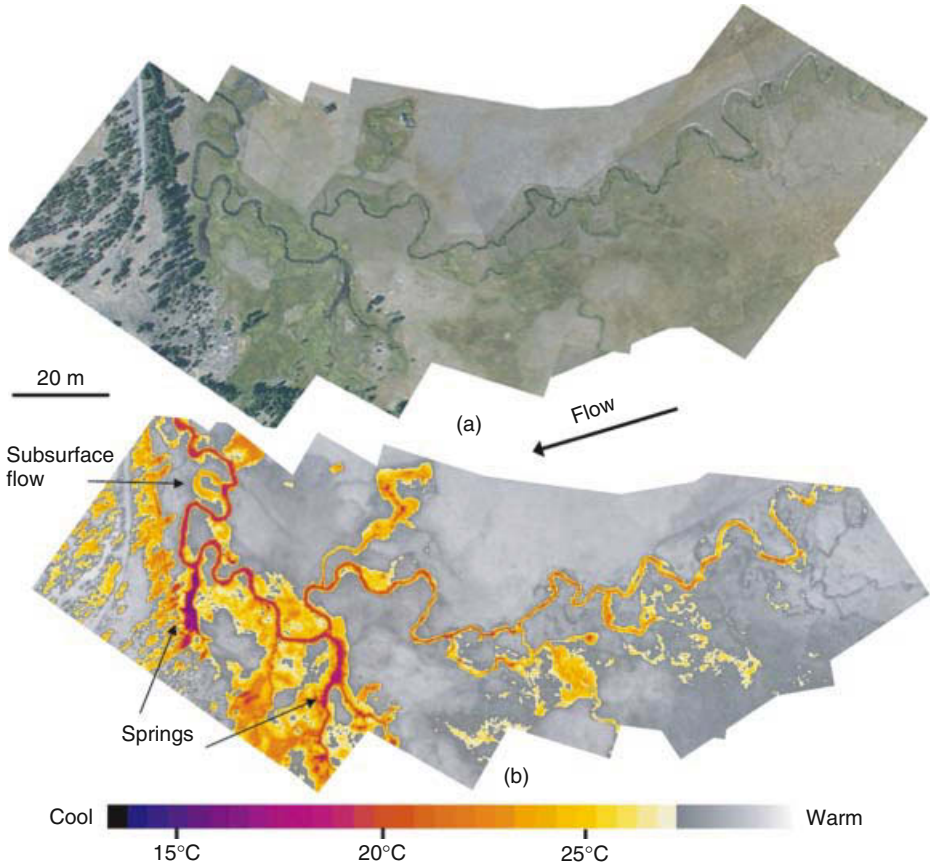

Figure 5.2 Natural-color (a) and airborne TIR (b) aerial images of groundwater springs flowing into the upper Middle Fork John Day River (Oregon, USA) in a montane meadow (16 August 2003). See Figure 5.1 for clarification of color and grayscale thermal classification. Complex subsurface hydrologic flow paths and areas of increased soil moisture adjacent to the wetted channel are revealed by lower TIR land and vegetation radiant temperature (United States Bureau of Reclamation, Dept. of Interior, USA; Watershed Sciences, Inc., Corvallis, Oregon, USA).

In the last decade, the increased awareness of TIR technology, combined with technological advances that have made TIR imaging systems more stable, portable, and affordable, has led to novel applications in riverine ecology. Both airborne- and ground-based approaches have proven highly effective for identifying and mapping the extent of very-fine resolution thermal heterogeneity associated with point sources, hyporheic flow, discharge patterns, and geothermal inputs within the river channel (Burkholder et al., 2008; Cardenas et al., 2008; Dunckel et al., 2009; Cardenas et al., in press). Other studies have utilised the entire swath width of TIR imaging systems to assess thermal variation beyond the river channel and across the floodplain and adjacent riparian areas (Rayne and Henderson, 2004; Arrigoni et al., 2008; Smikrud et al., 2008; Cristea and Burges, 2009; Tonolla et al., 2010).

Recent developments in TIR remote sensing of rivers have expanded the area of interest beyond water surface temperature – but there is much to be learned from viewing the entire 'thermal landscape' of rivers, laterally, longitudinally, vertically, and temporally. The vertical and temporal dimensions of thermal diversity in riverine systems have just begun to be investigated with TIR remote sensing. The vertical dimension, or thermal stratification, is poorly understood in TIR remote sensing because measurements of radiant temperature are made only in the surface layer of the water (approximately top 10 cm), which may not be representative of T_k further down the water column (this will be expanded on in a

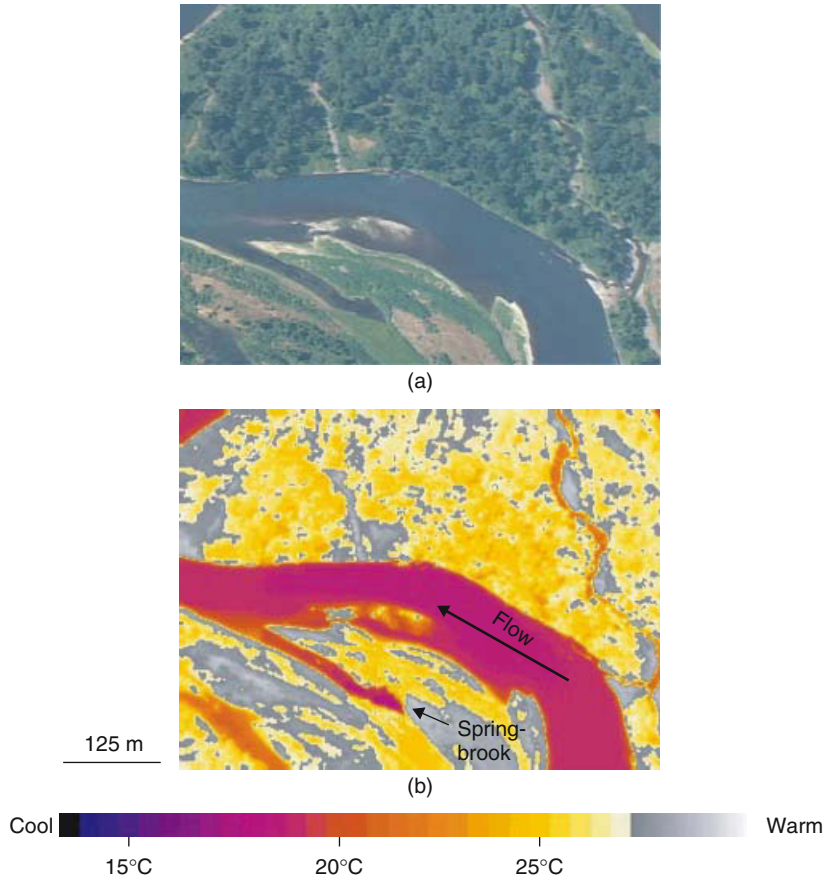

Figure 5.3 Natural-color (a) and airborne TIR (b) aerial images showing thermal heterogeneity in a complex floodplain of the Willamette River (Oregon, USA), which flows through a large, low-elevation agricultural valley (22 July 2002). See Figure 5.1 for clarification of color and grayscale thermal classification. Radiant water temperature varies laterally from the cooler and relatively homogeneous thalweg and main channel to warmer backwaters and disconnected channels. A springbrook is apparent where relatively cooler hyporheic flow emerges from the unconsolidated substratum of a large riverine island (Oregon Department of Environmental Quality 2006; Watershed Sciences, Inc., Corvallis, Oregon, USA).

later section). Where mixing in the water column occurs, cooler water can be detected at the surface, but few studies have determined *in situ* the necessary water velocities and fluvial morphology required to fully mix the vertical structure of the river. Further investigation of the vertical dimension may be conducted in winter when groundwater, which at this time is warmer than river water, is more likely to rise to the surface due to its lower density. Few studies have collected TIR images of rivers and streams in winter, but this area of inquiry holds much potential for quantifying surface water and groundwater interactions and identifying 'warm-water' refugia for fishes in cold regions (Tockner, 2006).

Comparisons of TIR images in rivers across seasons and years provides a means to assess changes in the thermal landscape associated with habitat degradation or to evaluate the effectiveness of floodplain restoration. The application of TIR remote sensing in restoration ecology of rivers is uncommon (for a notable exception see Loheide and Gorelick, 2006) but will likely gain momentum as rivers that were surveyed aerially in the 1990s are re-flown to monitor the effectiveness of management actions (e.g., channel modification and re-vegetation of riparian areas) at restoring thermal diversity in riverine landscapes. The following sections provide the technical context and practical applications of TIR remote

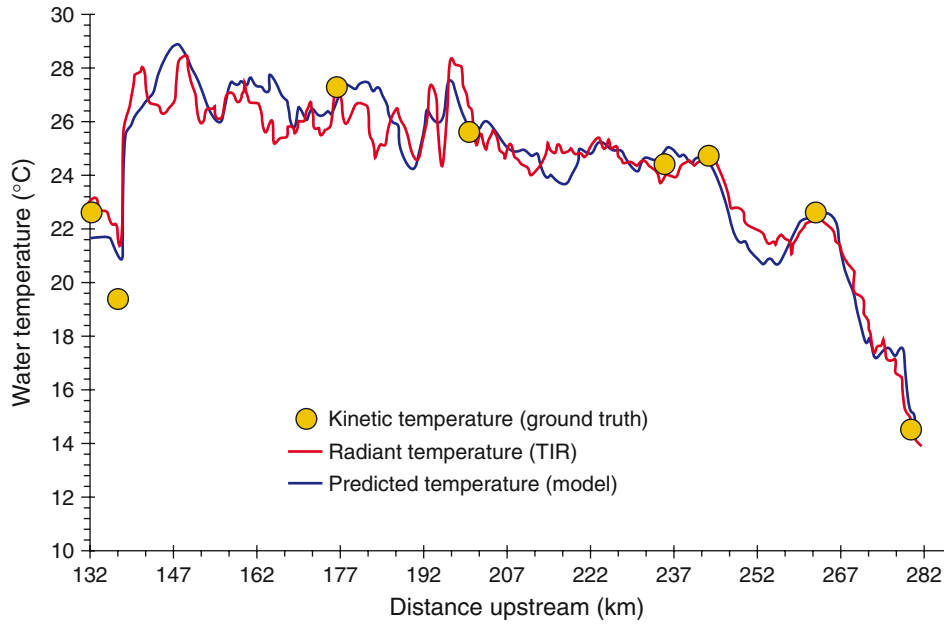

Figure 5.4 Longitudinal profile of water temperature in the upper Grande Ronde River (Oregon, USA) depicting radiant temperature acquired during an airborne FLIR overflight (20 August 1999), in-stream measurements of kinetic temperature, and calibrated model predictions. Distance upstream (x-axis) was determined from the river mouth (Oregon Department of Environmental Quality, 2010a, b).

sensing so that water resources managers and scientists can evaluate how this technology can be used both to address management needs in water quality assessment and biological conservation and also to further the understanding of hydrological processes and riverine ecosystems.

5.3 Technical background to the TIR remote sensing of water

This section focuses on the technical considerations necessary for informed planning and implementation of studies that use TIR remotely sensed images for monitoring streams and rivers. We therefore focus in this section, firstly, on the theoretical basis of the TIR remote sensing of water in general, and secondly, on the topics specific to the TIR remote sensing of riverine landscapes. We explicitly use the terminology of either the TIR remote sensing of *water* or of *rivers* to refer to whether the background applies to water in general, or to water in streams and rivers. A summary of the suggested processing required of TIR data to determine water temperature can be found in Figure 5.5. The theory of thermal properties of natural materials is extensively covered in the literature, and for the thermal remote sensing of water, specifically, we recommend a good introductory text (e.g., Mather, 2004; Lillesand et al., 2008) or overview (e.g., Atwell et al., 1971; Prakash, 2000).

5.3.1 Remote sensing in the TIR spectrum

All materials with a temperature above 0 K emit radiation, and as described by Wien's Displacement Law, the hotter the object, the shorter the wavelength of its emitted radiation. For example, the sun's temperature is approximately 6000 K, and the sun emits its peak radiation in the visible part of the electromagnetic spectrum (0.4–0.8μm) to which the human eye is adapted. Remote sensing in the region of visible, near infrared (NIR) and mid-infrared radiation (<3μm) utilises reflected radiation. In contrast, the earth's ambient temperature is ~300 K and its peak radiation is emitted at the longer wavelength of 9.7μm. Thermal remote sensing captures radiation emitted in these longer wavelengths (3–1000μm). As TIR observations are strongly affected by radiation absorbed

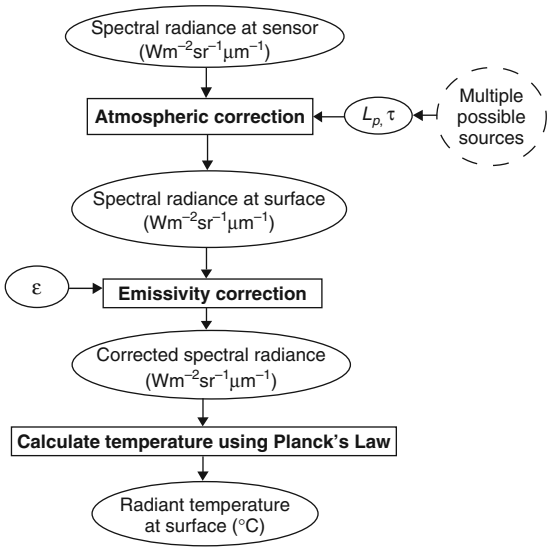

Figure 5.5 Flowchart summarizing the suggested processing of TIR data to determine stream temperature. See the Table of Abbreviations and text for definitions.

and emitted from water vapour, TIR applications focus on the 8–14μm region of the electromagnetic spectrum where atmospheric interference and contamination by solar radiation (in the 3–5μm region) is minimised.

5.3.2 The relationship between emissivity and kinetic and radiant temperature

A material's T_k is determined by the particular thermal characteristics of the material and its heat budget. In simplistic terms, this heat budget results from energy being absorbed, transmitted, and reflected, sometimes multiple times. For example, water has a high *thermal inertia*, which means that it changes temperature slowly as heat energy is added, a low *thermal conductivity*, which means that heat passes through it slowly, and a high *thermal capacity*, which means that it stores heat well.

Whereas the T_k of water can be measured directly using a thermometer that is in contact or immersed in the water, TIR remote sensing of water (using a radiant thermometer, or a ground-, air-, or space-borne imaging sensor) relies instead on indirect measurements of the radiation, emitted by the water body, to determine the water's radiant temperature, T_r. The amount and spectral distribution of this radiated energy is a combination of the material's T_k and its surface emissivity.

Emissivity (ε) defines the efficiency of a material at radiating energy compared to a blackbody. Emissivity values range from 0 to 1. A *blackbody* is a theoretical material with an emissivity of 1, which absorbs all incident radiation and re-emits it perfectly at all wavelengths. A *graybody* has an emissivity that is independent of wavelength λ and is <1. A *selective radiator* will have an emissivity that varies across wavelengths, and this characteristic can be used to identify the material based on its emissivity spectra. In the natural environment true blackbodies do not exist, which means that T_r will always be less than T_k.

Water can approximate a blackbody as its emissivity in the 8–14μm range is near 1 (Figure 5.6). There are many factors which influence water's actual emissivity. The emissivity of water can vary with the amount of suspended sediment (Salisbury and Aria, 1992), and dissolved minerals (e.g., as found in sea water). Features such as riffles and surface foam, which can roughen the water surface, will also alter the emissivity, as can physical characteristics such as wet rocks that have a different emissivity (closer to water) than dry rocks. As well as varying with wavelength, emissivity varies with the compound effects of both angular effects and the surface roughness. For large observation angles (>70° from nadir), rough water will have a higher emissivity than placid water at the same observation angle and will therefore appear warmer (Masuda et al., 1988). When the roughness of the water surface is constant, for small observation angles up to 30° there is a small decrease in spectrally variable emissivity and temperature (e.g., <0.1°C at 10μm for distilled water at 17.2 °C), but for observation angles >70° Fresnel reflection increases and the emissivity and T_r are significantly lower (Masuda et al., 1988; Ishiyama et al., 1995; Cuenca and Sobrino, 2004). In practical terms, providing the observation angles are within ~30° of nadir these effects are negligible.

The emissivity should therefore be chosen to match the specific water characteristics, and care taken in interpretation of TIR data under conditions which might change the emissivity. As the emissivity varies with wavelength, the emissivity should be matched to the band wavelength specifications of the sensor, and care should be taken when narrow-band temperatures are compared to temperatures obtained from sensors with different band characteristics.

The reflectivity of a material is the proportion of radiation incident upon it that is reflected back. There are a number of laws describing how energy is absorbed, transmitted and reflected, and for brevity we will only detail here with what is needed for applied TIR remote sensing

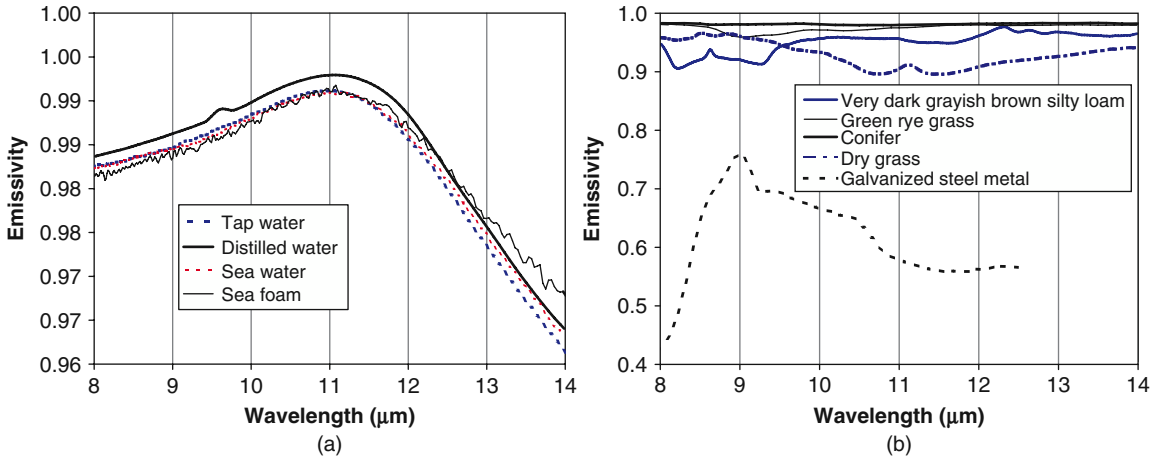

Figure 5.6 Emissivity in the 8–14 μm TIR region for (a) water and foam, and (b) other relevant materials. Note different scales for the x-axes ("Very dark grayish brown silty loam" [*85P3707*], green rye grass [*grass*], conifer [*conifers*], dry grass [*drygrass*], galvanized steel [*0525UUUSTLb*], tap water [*TAPWATER*], sea water [*SEAWATER*], and sea foam [*FOAM*] from the ASTER Spectral Library, Version 2.0 [*Baldridge* et al., *2009*]; distilled water [*WATER2_W*] from the MODIS Emissivity Library, 2010).

of rivers. As described by Lillesand et al. (2008), for most natural materials that are opaque to thermal radiation, Kirchhoff's Law describes how an object's emissivity and absorptivity are equal. Due to the conservation of energy, this can be written as:

$$\varepsilon(\lambda) = 1 - \rho(\lambda) \tag{5.1}$$

where $\varepsilon(\lambda)$ is the emissivity of the material at a wavelength λ, and $\rho(\lambda)$ is the reflectivity of the material. This relationship describes why water, for example, has a very low reflectivity across all wavelengths, and a correspondingly high emissivity. Equation (5.1) can also be used to determine an object's emissivity if its reflectivity in the TIR is known.

Good sources of reflectivity and emissivity data are spectral libraries, such as the MODIS Emissivity Library (2010) and the ASTER Reflectivity Library (Baldridge et al., 2009). Spectral libraries have the advantage of being measured under controlled conditions. Although the spectral libraries cannot cover all variations in emissivity described above, standard spectra for distilled water are usually suitable for the accuracy requirements of many applications which require T_r, including the TIR remote sensing of rivers. Emissivity and reflectivity spectra from a library also generally cover a range in wavelengths, with measurements at fine spectral intervals (e.g., 1 nm), and, if needed, the spectral data can be mathematically convolved to match the specific spectral characteristics of the data acquired for a given application.

5.3.3 Using Planck's Law to determine temperature from TIR observations

The radiant energy incident on a surface (e.g., sunlight) is termed its irradiance, while the radiant energy exciting the surface is its radiant emittance. The radiation emitted by an object is often assumed to be *Lambertian*, or emitting equally at all angles, although in practice water can be roughened by wind and waves and behave in a non-Lambertian manner. The radiant emittance is usually not measured across the whole hemisphere, but only from a particular direction and solid angle (measured in steradians, sr). For an assumed Lambertian surface, the radiation leaving the surface is assumed to be uniformly distributed across the hemisphere above the surface (which subtends 2π sr). When measured at a particular wavelength, the units of spectral radiant emittance are $Wm^{-2}\mu m^{-1}$.

Planck's Law describes the non-linear relationship of the total radiant emittance from a blackbody, at a particular wavelength, to its temperature. When expressed per unit wavelength, Planck's Law in simplified form (Mather 2004) is as follows:

$$W(\lambda, T) = \frac{c_1}{\lambda^5 (e^{c_2/\lambda T} - 1)} \tag{5.2}$$

where $W(\lambda, T)$ is the total spectral radiant emittance (i.e. not per unit of solid angle) at a particular temperature per unit area of emitting surface at wavelength (λ) in meters ($W\,m^{-2}\,m^{-1}$), T is the object's temperature in Kelvin, c_1 is $3.7242 \times 10^{-16}\,W \cdot m^{-2}$, and c_2 is $1.4388 \times 10^{-2}\,m\,K$. To

obtain an object's brightness temperature (i.e. without correcting for emissivity), we can invert Equation (5.2) as follows:

$$T(\lambda, W) = \frac{c_2}{\lambda \ln\left(\frac{c_1}{\lambda^5 W} + 1\right)} \quad (5.3)$$

To determine T_r rather than the brightness temperature from the measured TIR spectral radiance at a particular wavelength, we should first apply the emissivity correction (Equation 5.1) for W before calculating temperature using Equation 5.3. When implementing these equations, care needs to be taken with the units (e.g., wavelength is in m, not μm) and with the precision and number of significant digits for any computer software used in the calculation or else small errors in the calculation may be artificially magnified.

Note that while we describe here the general form of the corrections, they should be applied for individual bands and pixels, and adjusted according to the specific spectral characteristics of the sensor as described by its spectral response function. The band centre wavelength is generally used for calculations. An effective band centre for a sensor band can be determined by weighting all wavelengths within the defined sensor spectral band using for the band-specific spectral response function.

5.3.4 Processing of TIR image data

While some remote sensing data processing methods, such as geo-rectification, are common for all remote sensing data, the emitted nature of TIR remote sensing requires some different processing techniques compared to remote-sensing of reflected radiation. These special techniques will be described here, but for information on standard pre-processing, readers are referred to remote sensing textbooks (e.g., de Jong, et al., 2004; Mather 2004; Lillesand et al., 2008).

Required radiometric corrections of the data compensate for both the effect of the atmosphere on what is measured at the satellite, as well as between-image differences such as changes in the emissivity of the surface due to short-term factors such as wind blowing across the water surface. Radiometric corrections can be time-consuming and can be applied with different levels of processing depending on the application for which the data are to be used. To derive quantitative temperature values from raw TIR data requires either that a radiometric correction be applied to the data, or some form of other calibration data be used for an empirical correction (e.g., see Section 5.6.4 for an example with SSTs).

5.3.5 Atmospheric correction

While observations using TIR data focus on the atmospheric windows as previously described, water in the atmosphere between the water and the sensor is still one of the largest sources of error. For images acquired from a satellite in earth orbit, the sensors are recording at the top of the atmosphere (TOA) and therefore observe the radiation originally emitted from the earth's surface (i.e. L_g) after it has passed through the atmosphere. This emitted spectral radiance measured at the sensor (L_s) is influenced by many factors related to its path through the atmosphere and factors such as the viewing geometry of the sensor and sun. These factors can be summarised by two factors: an additive spectral radiance contribution (i.e. path radiance, L_p) resulting from upwelling spectral radiance contributed by the atmosphere, and a multiplicative factor (i.e. transmissivity, τ) which is due to the attenuation by atmospheric absorption and scattering of spectral radiance emitted by the surface and not reaching the sensor. The correction of L_s to determine L_g is as follows:

$$L_g(\lambda) = \frac{L_s(\lambda) - L_p(\lambda)}{\tau(\lambda)} \quad (5.4)$$

where:

L_g = land-leaving spectral radiance at a particular wavelength ($Wm^{-2}\mu m^{-1}sr^{-1}$)
L_s = sensor spectral radiance ($Wm^{-2}\mu m^{-1}sr^{-1}$)
L_p = path spectral radiance ($Wm^{-2}\mu m^{-1}sr^{-1}$)
τ = transmissivity (unitless)
λ = is the wavelength of the sensor (e.g., the band centre wavelength)

To determine L_g from L_s accurately it is essential to correct for atmospheric conditions as even on clear days there will be an effect from atmospheric gases and water vapour. Smoke, dust or haze can result in large effects. TIR radiation also cannot be sensed through clouds or fog, so standard remote sensing practices should be used to identify and mask these in the image. Once L_g has been determined from L_s using Equation 5.4, T_r can be determined using Equation 5.3.

L_p and τ can be determined for the specific image date using a radiative transfer model such as MODTRAN (Berk et al., 1989), 6S (Kotchenova, et al., 2006), or FLAASH (Adler-Golden et al., 1999) to calculate all aspects of scattering and transmission of radiance through the atmosphere. However, such models are time-consuming and require input data which may not be available real-time,

such as vertical profiles of atmospheric water vapour. Some of these parameters can be estimated from standard atmospheres or models. For example in a study of TIR remote sensing of streams and rivers in the USA (Handcock et al., 2006), a radiosonde was launched on a weather balloon concurrent with sensor overpasses, and L_g and τ were determined for each image using the Penn State/NCAR mesoscale model (MM5) (Dudhia, 1993). The MM5 column atmospheric water vapour or radiosonde profile water vapour was used as an input to radiative transfer modeling (MODTRAN 4.0, Berk et al., 1989; Ontar Corporation, 1998) to determine the spectrally varying atmospheric τ and L_p to correct each image (Kay et al., 2005).

While critical to accurately retrieving temperature from TIR data, atmospheric correction can be time consuming and expensive. An alternative is to use non-atmospherically corrected water temperature data to assess relative spatial patterns within a single image. The assumption is made that if a single uniform atmospheric correction had been applied across the whole image then its quality only affects the absolute accuracy and not the uncertainty of remotely sensed river-temperature measurements. The resulting relative temperatures can be used along with image interpretation of the river with its terrestrial and aquatic context for applications where knowing absolute temperatures is not critical. For example, to identify hydrological features such as seeps (e.g., Figure 5.1), confluences of streams or rivers with contrasting temperatures (e.g., Figure 5.7), as well as thermal refugia or possible pollution sources. In some situations having absolute temperature is still essential, such as mapping thermal characteristics of fish habitat.

5.3.6 Key points

- Interpretation of TIR image data to determine water temperature can be complex. However, understanding

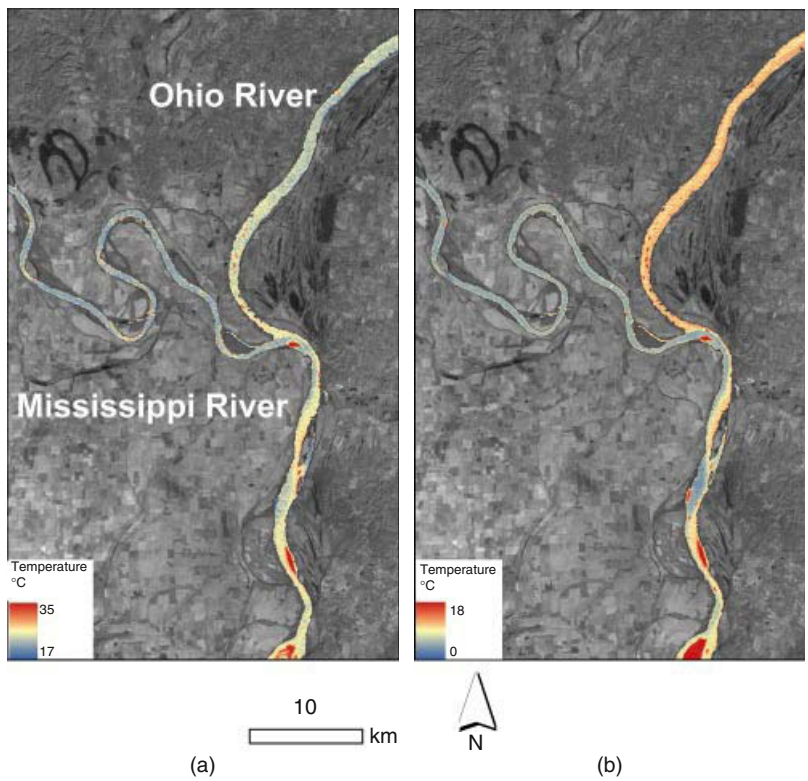

Figure 5.7 Confluence of the Mississippi and Ohio rivers in (a) September 2001 and (b) November 2001 as viewed in Landsat 7 ETM+ images. Monitoring bulk river temperature in this region is complicated by the mixing of cooler water from the Mississippi River and warmer water from the Ohio River, which continues to affect downstream temperature for more than 10 km.

this theoretical background is necessary for choosing whether the required tools and technical skills are available to process and interpret the images.

- Emissivity should be chosen to match the specific water and sensor characteristics. Spectral libraries provide a good source of emissivity and reflectivity data for most applications. Care must be taken in interpretation of TIR data under conditions that might affect the emissivity, such as large observation angles and rough water.
- To reduce errors that can occur at large observation angles, images should be chosen to be near nadir ($<30^{\circ}$). When multiple images are obtained they should have similar observation angles.
- While critical to accurately retrieving quantitative temperature from TIR data, radiometric correction can be time consuming and expensive. An alternative is to use non-radiometrically corrected TIR images to assess relative spatial patterns within a single image, but this will limit the applications for which the data can be used to those not requiring absolute temperature information.
- TIR radiation cannot be sensed through clouds or fog, so standard remote sensing practices should be used to identify and mask these out of the image before quantifying water temperature.
- See also Table 5.1.

5.4 Extracting useful information from TIR images

Once the TIR image data have been processed to determine T_r, it is still necessary to extract information specific to the thermal application. In this section we first discuss how to calculate a representative water temperature. We then examine how both the size of the river relative to the pixel size of the TIR imaging sensor, and the near-band environment, influences the accuracy of extracted water temperature. We note that care is required for interpretation of TIR images within their terrestrial and aquatic context; a trained operator is required to reduce errors associated with image interpretation. A detailed examination of this topic is beyond the scope of this chapter, therefore we illustrate this complexity with examples.

5.4.1 Calculating a representative water temperature

Thermal applications usually require fine resolution TIR data to map thermal pollution sources or locate thermal refugia. Extracting a longitudinal water temperature profile can be complex because temperature from the stream or river centre may not be representative spatially across the stream. This necessitates approaches such as weighted averages (Cristea and Burges, 2009) or median filtering (Handcock et al., 2002).

Many TIR imaging sensors used for measuring water temperature are designed to have multiple spectral bands located at different wavelengths. These wavelengths are typically determined from the TIR emissivity spectra useful for geological applications (e.g., Gillespie et al., 1984; Bartholomew et al., 1989). When available, multiple bands have an advantage for checking the accuracy of image processing when ground-based temperatures are available, because of the physical constraint of there being only one true temperature. The band or bands with the least amount of instrument noise and atmospheric effects can then be selected to calculate the final image temperatures. Alternatively, multiple bands can be averaged to reduce noise due to atmospheric or sensor differences and provide a better estimate of the actual temperature (Handcock et al., 2006).

5.4.2 Accuracy, uncertainty, and scale

The issue of spatial scale is critical to the remote sensing of rivers using TIR data, as the combination of river width and pixel size will determine whether it is possible to distinguish the river from the bank at the desired levels of accuracy and uncertainty with the TIR imaging sensor. The accuracy (bias) of a TIR measurement can be compared to a known *in situ* reference value used for validation, while its uncertainty (precision) is the repeatability of measurements. The radiometric precision of a TIR sensor is described by its NEΔT, or 'noise-equivalent change in temperature,' which is the minimum difference in temperature that the sensor can resolve as a signal from the background noise.

Rivers often have a complex morphology of channels, boulders, shallow areas, gravel bars, islands and in-river rocks, and vary greatly in hydrological and hydraulic characteristics such as ground-water inputs, water depth, water velocity and turbulence fluctuations. Handcock et al. (2006) quantified the accuracy and uncertainly related to the TIR remote sensing of river temperature across multiple spatial scales, imaging sensors, and platforms, and showed that when the water was resolved by less than three pure water pixels of a well-mixed river, the measurements had low accuracies and high uncertainties.

In practice, it can be difficult to find three pure water pixels as the edge pixels are frequently contaminated

by bank material. TIR remote sensing of water involves a trade-off between having a pixel size fine enough to identify spatial patterns and reduce mixing with bank materials, and coarse enough so that the cost of flying large areas is not prohibitive. TIR satellite-based images generally cover large areas (e.g. ASTER images cover a ground area of 3600 km^2 and Landsat ETM^+ ~34200 km^2), but their pixel sizes are commonly too coarse to resolve the river channel, except for the widest rivers. However their low cost, capability for regional coverage, and the potential for repeat monitoring with systematic image characteristics, make satellite-based TIR imaging sensors attractive if the pixel size is suitable for the river size. Airborne- and ground-based platforms produce TIR images with finer pixel sizes suitable for narrower rivers. Ground based TIR imagery can also be limited by the difficulty in locating sites suitable for the operation of the TIR sensor at an elevation above the water to resolve significant amounts of the stream channel. Further discussion of the characteristics of different sensor platforms can be found in Section 5.5.

For pixels that are not pure, such as for edge pixels that are a mixture of the bank and water, either a single emissivity needs to be assumed for the pixel, resulting in additional error for the temperature estimation for the pixel, or some method needs to be used to unmix the pixel. For example, the pixel can be unmixed using a spectral mixture analysis (Gillespie, 1992; Gustafson et al., 2003; Sentlinger et al., 2008, Gu et al., 2008).

5.4.3 The near-bank environment

The near-bank environment includes objects with a wide variety of temperatures and emissivities. It includes bark, branches, grasses, leaves, soil, sand, and rocks. Depending on the season, the time of day, and whether the near-bank objects are shaded, they may be warmer or cooler than the water. For example, for summer day-time observations, sun-lit rocks and woody debris exposed during low water levels could be warmer than the water. In comparison, a gravel-bar shaded by the trees could be cooler than adjacent water and would be confused with cold water inputs, as could riparian vegetation cooled by evapo-transpiration. These examples illustrate the sort of complexities found in image interpretation of TIR images in a riverine landscape.

Emitted radiation from the near-bank environment of vegetation and rocks can reach the sensor directly or be scattered from the river surface as the result of emission, reflection, and multiple-scattering of emitted

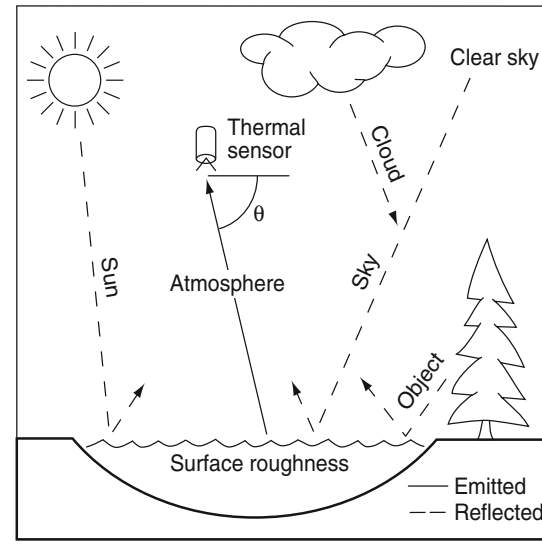

Figure 5.8 Sources of emitted and reflected TIR radiation in thermal remote sensing of rivers and streams (Torgersen et al., 2001, Figure 1). Reprinted from *Remote Sensing of Environment*, **76**(3), Torgersen, C.E. et al., Airborne thermal remote sensing for water temperature assessment in rivers and streams, pp. 386–398, Copyright 2001, with permission from Elsevier.

radiation (Figure 5.8). TIR radiation emitted from near-bank objects may pass directly into the path of the sensor, resulting in erroneous image interpretation, particularly when the bank material's temperature is very different from the water temperature. This is particularly problematic for ground-based TIR imaging sensors observing the water from the bank with a large observation angle (e.g. Handcock et al., Figure 7b, 2004; Cardenas, et al., Figure 2, 2008). TIR radiation emitted from near-bank objects may also be scattered or reflected from other surfaces into the sensor, both of which will increase the measured T_r. This multiple scattering effect is small compared to the temperature of the water. For example, for a tree with a temperature of 25 °C and water at 17.2 °C there is a calculated increase in the observed water temperature of 0.10 °C–0.65 °C, respectively, depending on the viewing geometry (Handcock et al., 2006). When the bank vegetation is tall compared to the width of the river it may not be possible to find regions in the river centre that are not contaminated by scattered radiation emitted by the bank vegetation. In situations where it is difficult to obtain pure-water pixels, higher resolution imagery may be needed, and more than 10 pixels may need to be sampled from the imagery to resolve T_r accurately (Torgersen et al., 2001).

5.4.4 Key points

- Depending on the TIR sensor and platform that is used, the available TIR data must be matched to the size of the river being monitored; as a general rule, when the channel width is resolved by fewer than three adjacent pure water pixels in a well-mixed river, the measurements will have low accuracies and high uncertainties. In most situations, more than 3 pixels will be needed. Similar accuracy problems would be expected when resolving other water bodies.
- TIR radiation emitted from near-bank objects may pass directly into the path of the sensor, resulting in erroneous image interpretation, particularly when the bank material's temperature is very different from the water temperature.
- Having multiple spectral bands is an advantage where there is a single known temperature, which can be used as a check of the accuracy of the data processing.
- Care must be taken to interpret images within their terrestrial and aquatic context.
- See also Table 5.1.

5.5 TIR imaging sensors and data sources

In this section, we discuss sources of TIR data, focusing on image-based sensors rather than point-based sensors such as radiant thermometers. Point-based sensors are discussed in the next section in relation to TIR validation. There are many sensors for measuring TIR data, and their availability and refinements is changing rapidly. This chapter does not attempt to provide a comprehensive overview. Instead, some examples of particular sensors are used to illustrate the characteristics typical of particular types of sensors. Common to all sensor platforms is the issue of calibration. Some TIR imaging sensor systems have on-board calibration sources, typically a hot and a cold calibration source. Other systems record only relative values of emitted radiation, or digital numbers (DN), and must be calibrated (see Section 5.6 for methods of measuring *in situ* water temperature).

5.5.1 Ground imaging

There are many examples of ground-based imaging systems that provide an array of TIR measurements. When choosing a TIR imaging sensor, specifications are usually given as to its pixel size and precision. Pixel sizes from such imaging systems will be determined by the distance between the sensor and the water, and are typically <1 m. Many ground-based TIR imaging systems are available, including forward looking infrared (FLIR) imagers (Rogalski and Chrzanowski, 2002) that can be used in both ground-based and airborne surveys. High quality systems have NEΔT values of 0.1 $^{\circ}$C or better.

When using ground-based TIR imaging sensors, care must be taken with the viewing geometry of the sensor relative to the water and the surroundings. In particular, tall near-bank objects such as trees will scatter emitted radiation onto the water, and some of this radiation will be reflected back into the field of view (FOV) of the imaging sensor (see Section 5.4.3 for more details). Data from ground-based imaging sensors such as a FLIR can be calibrated (e.g., Handcock et al., 2006) using shielded and stirred water targets at different temperatures. Linear regression is used to relate raw image values (DN) to T_r measurements made using a hand-held broadband radiometer.

5.5.2 Airborne imaging

As airborne TIR imaging sensors are widely used for monitoring of water temperature in riverine environments, we will cover the topic in some detail. Airborne TIR imaging sensors can be mounted on either fixed-wing aircraft or on a helicopter which may be manned or unmanned. The resulting pixel size of the TIR data (instantaneous field of view, or IFOV) is a function of the distance from the water surface (determined by the height that the platform flies), the sensor characteristics, and the optical FOV of the sensing system. The height of the platform and optical FOV also determines the ground footprint of the resulting image.

The narrow swath widths of TIR images from airborne platforms – typically from a few kilometers for fine resolution images, to a few 10s or 100s of meters for very-fine resolution images – reduces their ability to capture long stream reaches as the channel winds in and out of the preferred straight-line flight pattern. To best manage the issues of edge pixels (discussed in Section 5.4.2) in airborne TIR image acquisition, a balance must be struck between the resolution of the sensor, the desired resolution of the image, the width and sinuosity of the stream channel, and the altitude of the aircraft. Finer pixel sizes may be obtained from the same sensor when the aircraft is flown at lower altitudes, however, as the number of times the aircraft is required to circle around and line-up on a new straight-line for acquisition of the stream channel,

the longer and more expensive the image acquisition will become.

Another important consideration for airborne data acquisition is that the images do not provide a truly synoptic assessment, or 'snapshot', of water temperature at a specific time if the images are collected sequentially along the river course. Thus, diurnal changes in water temperature should be considered in planning airborne data collection. See further discussion of this topic in Section 5.5.2.1 on helicopter versus fixed-wing aircraft, and Section 5.6 on the validation of temperature measurements.

The selection of an airborne platform/TIR-imaging-sensor depends on project-specific details such as the river characteristics (size, sinuosity, etc.), temporal constraints, desired spatial and thermal resolutions and accuracies, and map accuracy specifications. TIR imaging systems have evolved continually with advances in technology, and there are a number of TIR imaging sensors available on the market suitable for use on airborne-platforms. These TIR imaging sensors have unique technical characteristics such as physical size, temperature resolution, integration times, detector types and sizes, and optics. However, there are also common features that make these TIR imaging sensors suitable for TIR remote sensing of water.

TIR imaging systems must be able to store raw DN that can be converted either internally or during post-processing to a measure of radiant energy. Manufacturers differ in how this is accomplished, but in most cases the detectors are calibrated in the laboratory environment against a black-body source and this information is stored (either internally or externally) as a conversion curve that is unique to the sensor. Because airborne remote sensing typically involves collecting sequential frames, another important sensor system characteristic is its ability to retain internal radiometric consistency throughout the data acquisition. Although conditions such as ambient temperature change, the TIR imaging system must be able to control or minimise internal drift such that frame-to-frame measurements are consistent. TIR imaging sensor manufacturers accomplish this in a number of ways such as using internal temperature references or cooling mechanisms which retains stability in the detector array. Finally, the TIR imaging system must account for radiometric distortion due to variability in individual detector response and lens optics (in the case of frame based TIR imaging sensors). This is referred to as uniformity correction and can be accomplished either internally or during the post processing.

A wide variety of TIR imaging sensors have been used for airborne applications. For example, in one study (Handcock et al., 2006) the MODIS/ASTER (MASTER) sensor (Hook et al., 2001) was flown on a King Air B200 fixed-wing aircraft at altitudes of ~2000 and ~6000 m, which gives approximate pixel sizes of 5 and 15 m, respectively. The MASTER sensor has ten TIR bands (10.15–11.45μm) with an NEΔT that ranges from 0.46 to 0.71 °C, and can scan ±43° from nadir. In another example, on Prince Edward Island (Canada), a FLIR Systems SC-3000 TIR imaging sensor mounted on a Cessna 172 fixed-wing aircraft was used to acquire images of the Trout River. These data were successfully used to detect and quantify ground water discharge to the estuary (Danielescu et al., 2009). The SC-3000 sensor has a single TIR band of 8–9μm with a NEΔT of 0.02 °C. The sensor has a fixed horizontal FOV of ±10° from nadir and a detector array of 320 × 240 pixels. In this study, the aircraft was flown at an altitude of 1000 m to give a ground sample distance (GSD, i.e. the pixel size of the imaging sensor expressed in ground units) of 1 m. Although the term GSD is often used interchangeably with pixel size, it is sometimes expressed explicitly when the ground distance represented by a pixel changes across the image, which is common for aerial imaging and oblique view geometries. In Northern Utah, a helicopter-mounted Space Instruments Firemapper 2.0 was used to collect TIR images with a 3 m GSD to identify areas of thermal refugia in the 9.6 km^2 Cutler Reservoir (Dahle 2009). The Firemapper 2.0 system has a single TIR band of 8–12μm with an NEΔT of 0.07 °C. The imaging sensor has horizontal FOV of ±22.1° from nadir and a detector array of 320 × 240 pixels.

Early work with airborne TIR imaging in riverine environments focused primarily on detecting cold water sources and longitudinal temperature patterns (Torgersen et al., 1999, 2001) with data geo-referenced to specific locations along the longitudinal extent of the river (i.e. tributary junctions, springs geo-referenced according to their distance upstream). Over the past decade, creating continuous image mosaics with specified mapping accuracy has increasingly become a requirement so that the image data can be accurately combined with other spatially explicit data layers and accurately geo-referenced field data. Although some of the early TIR images were from ground-based imaging sensors mounted on an aerial platform, more recent TIR sensor systems such as the ITRES TASI 600 (USA) push-broom hyperspectral thermal imaging sensor system are specifically designed for airborne operations. Such imaging sensors provide

timing and scan information suitable for integration with airborne Global Position System (GPS)/inertial measurement units (IMU) for direct geo-referencing. Similarly, the FLIR Systems SC6000 QWIP frame based sensor (8–9.2μm) has accurate timing and triggering capability that allow direct integration with an aircraft's modern GPS which records its geographical location, and its IMU which record the aircraft's velocity, orientation, and gravitational forces. An IMU greatly simplifies the process of extracting ground control points (GCPs) used for orthorectification of the image data. When an IMU is not available, as is more common in older systems, these GCPs need to be extracted from other image sources, base-maps, or manual or surveyed GPS locations. The process of identifying GCPs in the image is simplified when a concurrent visible image is obtained with the TIR image, otherwise distinguishing water from the bank material can be difficult when, for example, a shaded gravel bar is colder than water and confused for a cold-water spring, or dead wood in the stream is confused for a warm water input.

TIR imaging systems have progressively increased the size of the detector arrays, allowing a broader range of options for smaller GSDs or larger ground footprints at fine and medium pixel sizes. In general, this also allows a broader range of platform options since fine-resolution pixel sizes that were once achieved from a helicopter can be designed for higher flying aircraft capable of covering greater areas in shorter amounts of time. For example, the FLIR Systems SC6000 offers multiple lens options, has a pixel array of 640 × 512, and an NEΔT of 0.035 °C. With a ±17.5° FOV (25 mm lens), a 1 m pixel can be achieved with a 644 m wide ground footprint. The previously mentioned ITRES TASI 600 is a pushbroom hyperspectral thermal imaging sensor that acquires an image with 600 pixels across its track with a ±20.0° horizontal FOV and 32 bands within the 8–11.5μm spectral range (the advantage of multi-band thermal imaging sensors was discussed in Section 5.4.1). Finally, technological advances have made small, relatively inexpensive handheld thermal imagers appealing for mounting on airborne platforms. However, these image systems typically do not have the radiometric features or durability suitable for the airborne environment.

5.5.2.1 Helicopter versus fixed-wing aircraft

TIR imaging sensors have been mounted on both helicopter and fixed-wing airborne platforms. The selection of platform depends in a large part on the objectives of the data acquisition, the desired TIR imaging sensor spatial resolution, and the characteristics of the river.

The advantage of a fixed-wing aircraft is that the post-processing of TIR images is simplified by the relative stability of the platform, whereas a helicopter will typically have more variable flight characteristics such as altitude, yaw, roll, and pitch, which require additional processing and can introduce artifacts into the image which makes image interpretation more complex. Fixed-wing aircraft have long been used for aerial photography and other airborne remote sensing tasks. Consequently, finding a commercial charter for a fixed-wing aircraft with an existing camera port and appropriate flight characteristics, which is also located close to almost any project site, is relatively straightforward. Additionally, the instrumentation on fixed-wing aircraft is normally located inside the aircraft so that the installation, operation, and transport of the sensor is simplified when compared to operating from a helicopter. On rotary-winged aircraft, the instrumentation is most often external to the aircraft in a weatherised pod. In general, helicopters have a smaller range and higher operating costs than fixed-wing aircraft, but are more suitable for certain data-collection missions.

Fixed-wing aircraft are generally preferred in TIR image collections where flight parameters (altitude, speed) can remain relatively constant over the project area, such as for large water bodies or targeted sections of river with limited terrain relief. Helicopters are more suitable for collecting images along a sinuous corridor at very fine resolutions where the helicopter's slow speed and maneuverability are an advantage, and the acquisition of ultra-high resolution images is needed (e.g. for studying complex braided floodplains). In many cases, a fixed-wing aircraft may have to collect multiple lines of image data to capture the same areas, and may be unable to safely maneuver at the low altitudes required to capture images of the same spatial resolution.

As TIR imaging sensor systems decrease in size and cost, their application from airborne platforms is likely to increase. Smaller TIR imaging sensors can also be mounted within unmanned aerial vehicles (UAVs), including remotely controlled aircraft (e.g., Berni et al., 2009) and under balloons (N. Bergeron, Institut National de la Recherche Scientifique, Quebec, Canada, pers. comm.).

5.5.2.2 Airborne image analysis

Some of the factors and considerations of using TIR imaging sensors on airborne platforms, and their

post-processing, applies also to other remote imaging sensors; thus, standard methods can be used. Airborne data also need to be calibrated. For example, as described previously in Handcock (2006), the flight team for the MASTER multispectral data collection processed the TIR data to 'radiance-at-sensor.' using onboard calibration targets and an onboard GPS to record the aircraft's location. Ground-based data can also be used to calibrate raw TIR data, as will be explored in Section 5.6.

If the objective is to create continuous image mosaics of riverine systems or large water bodies, the acquisition of overlapping images becomes especially important, as does the timeliness of image acquisition (see Section 5.6.1). The ability to capture images efficiently at fine spatial resolutions, particularly on smaller streams, is paramount to minimising the diurnal change in water temperature during the image capture. For example, a recent 48 km stretch of the Anchor River (AK, USA) was flown by helicopter in 0.6 hr at a spatial resolution of 60 cm GSD. A flight plan for the same corridor, using a fixed-wing aircraft at the same GSD, would have required a flight time of approximately 2.4 hr.

5.5.3 Satellite imaging

Space-borne TIR imaging sensors can cover a greater aerial extent than airborne TIR imaging sensors and cover a range of pixel sizes, number of bands, FOV, revisit times, and sensor sensitivities. If TIR satellite images are available for the study time, and are of a suitable pixel size compared to the thermal application (see Section 5.4.2), they can be an attractive source of broad-scale data due to their low cost, capability for regional coverage, and the potential for repeat monitoring with systematic image characteristics. While TIR satellite-based images generally cover large areas, their coverage may still not be extensive enough to fully track some water bodies. Therefore, measurements of long channel reaches may have to be compiled over several days or weeks depending on the satellite orbit.

TIR imaging sensors typically have larger pixel sizes than do visible and near infrared (VNIR) imaging sensors, with the pixel size being determined by the sensor specifications (e.g., aperture, sensitivity of the detector, and the desired NEΔT). For example, the Advanced Spaceborne Thermal Emission and Reflection (ASTER) radiometer (Kahle et al., 1991; Yamaguchi et al., 1998), mounted on NASA's Terra spacecraft, has a VNIR sensor with three bands (15 m pixel size), a shortwave infrared (SWIR) sensor with six bands (30 m pixel size), and a TIR sensor with five bands (8.12–11.65μm) with 90 m pixel size and an NEΔT of $\leq$0.3 °C at 27 °C (Gillespie et al., 1998; Yamaguchi et al., 1998). While the pixel size of the ASTER TIR sensor is fine in terms of a satellite-based imaging sensor, it is 'medium' based on the multi-sensor criteria defined previously. The revisit time for ASTER is 16 days, and the FOV of the system is 60 km. As well as raw TOA ASTER data which are not radiometrically corrected, a number of higher-level products have been are available, including temperature, emissivity, and ground-leaving spectral radiance.

The NASA EOS MODIS sensor is also on the Terra platform (imaging in the morning), as well as a second MODIS sensor onboard Aqua (imaging in the afternoon). MODIS has ten TIR bands (6.54–14.39μm) with a pixel size of 1000 m and an estimated NEΔT of 0.05 °C at 27 °C (Barnes et al., 1998). Although MODIS has more bands than ASTER and a wider FOV (2330 km), the larger pixels limits it to observations of wide rivers. One advantage of MODIS is that images of the entire globe are acquired daily (and more frequently for higher latitudes). As well as raw TOA MODIS that have not been radiometrically corrected, a number of higher-level products are available, including temperature and emissivity.

The Landsat ETM$^+$ sensor on Landsat-7 is in the same orbit as Terra, which allows images to be acquired ~20 min apart with a 16-day revisit time. The single TIR band of Landsat ETM$^+$ (10.40–12.50μm) has inherent pixel size of 60 m (National Aeronautics and Space Administration, 1998), which is more recently available resampled to 30 m for easier comparison with other Landsat bands. The NEΔT of the Landsat ETM$^+$ TIR band is 0.22 °C at 7 °C (Barsi et al., 2003), and the FOV of the system is 185 km. The TIR sensor on Landsat was historically not always switched on to acquire data; however, the large number of images in the Landsat archive, the ongoing acquisitions, and the recent availability of free data, makes Landsat TIR an attractive option if it meets an application's specifications.

5.5.4 Key points

- The choice of TIR imaging sensor and whether the platform is ground-, air-, or satellite-based will depend on many factors, including the size of the area that has to be covered, how frequently data are required, cost and sensor availability, and whether the accuracy requirements of the application require a TIR imaging sensor with on-board calibration sources.

- Ground-based TIR imaging sensors are convenient but can only view the water from specific locations along the stream. Observation angles need to be chosen carefully to reduce the effects of scattering from bank objects.
- Airborne TIR imaging sensors provide spatially extensive images with fine pixel-sizes suitable for narrow streams and rivers, but acquisition can be costly, processing complex, and images are generally acquired over narrow swath widths.
- The pixel size and ground footprint of the TIR image is a function of the altitude above the water body at which the sensor collects data, the sensor characteristics, and the optical FOV of the sensing system.
- A balance must be found between the pixel size of the TIR sensor and the altitude at which airborne images are collected. Too high an altitude will result in more problems with mixed pixels, while too low an altitude will increase the expense and time required to acquire images over a given area.
- Advantages of fixed-wing aircraft include the relative stability of the platform that simplifies post-processing of TIR images, and the lower operating costs.
- Advantages of rotary wing aircraft include the greater flexibility of the platform for tracking sinuous riverine features and for flying at the low altitudes required for capturing very-fine resolution imagery. Such advantages require additional processing, and can introduce artifacts into the image which may make image interpretation more complicated, but software advances will likely reduce these disadvantages in time.
- UAVs hold great potential for future collection of TIR imagery, however, the lack of defined operating rules and licensing procedures for most countries severely limits their usage.
- Space-borne TIR imaging sensors provide spatially extensive images for low cost over large areas, but pixel-sizes are usually coarser than airborne data and are commonly too coarse to resolve the river channel, except for the widest rivers. However their low cost and capability for regional coverage at multiple points in time make satellite-based TIR imaging sensors attractive if the pixel size is suitable for the river size.
- The typically narrow swath widths of airborne TIR images make it more likely that overlapping scan lines must be collected and processed to create a mosaic of the river.
- Common to all sensor platforms is the issue of calibration. Some TIR imaging sensor systems have on-board calibration sources, while other systems record only relative values and must be calibrated.

5.6 Validating TIR measurements of rivers

5.6.1 Timeliness of data

Water temperature in streams and rivers changes throughout the day as the sun elevation angle and heating changes. Collecting validation data for TIR observations requires that water temperature measured is close enough to the time of the TIR image collection that the temperature has not changed significantly. This can be relatively easy to do in the case of ground-based images but is much more complex for observations from aircraft or satellite. In all situations, the collection of simultaneous measurements can be difficult due to the requirement for large numbers of personnel. Two questions that must be addressed pertain to the time of day of image capture and the duration of the collection period, both of which depend on the application. For example, to detect warm groundwater springs during winter, TIR images should be obtained when the river is the coldest.

If multiple images are to be compiled into a mosaic to provide coverage for a larger area, TIR data should be acquired when water temperature is most stable. River temperature is typically most stable in the early afternoon when air temperature is also relatively stable. However, the thermal inertia of the river water provides additional stability not found in air temperature, increasing the time over which river conditions should reflect the thermal conditions during TIR image acquisition. To study this question more closely, we have provided observations acquired at an interval of 15 min from four sites in the Pacific Northwest (USA) (Figure 5.9). Two sites are on a large river (Green River, annual flow 45.6 $m^3 s^{-1}$), whereas the other two are on smaller streams (Big Soos Creek, annual flow 3.5 $m^3 s^{-1}$; and a tributary to Covington Creek, which is a tributary to Big Soos Creek). Two sites are relatively open with limited riparian cover, whereas the other two have dense riparian cover (the tributary to Covington Creek is almost completely shaded). All four sites show a strong diurnal cycle, with minimum temperature occurring just as the sun rises above the horizon, and maximum temperature occurring by late morning or early afternoon. Changes in temperature are typically slowest around these extremes, so that early morning and early afternoon have the widest sampling windows with the least change in temperature. The width of a sampling window is highly dependent on how much of a change in temperature is acceptable. If observations

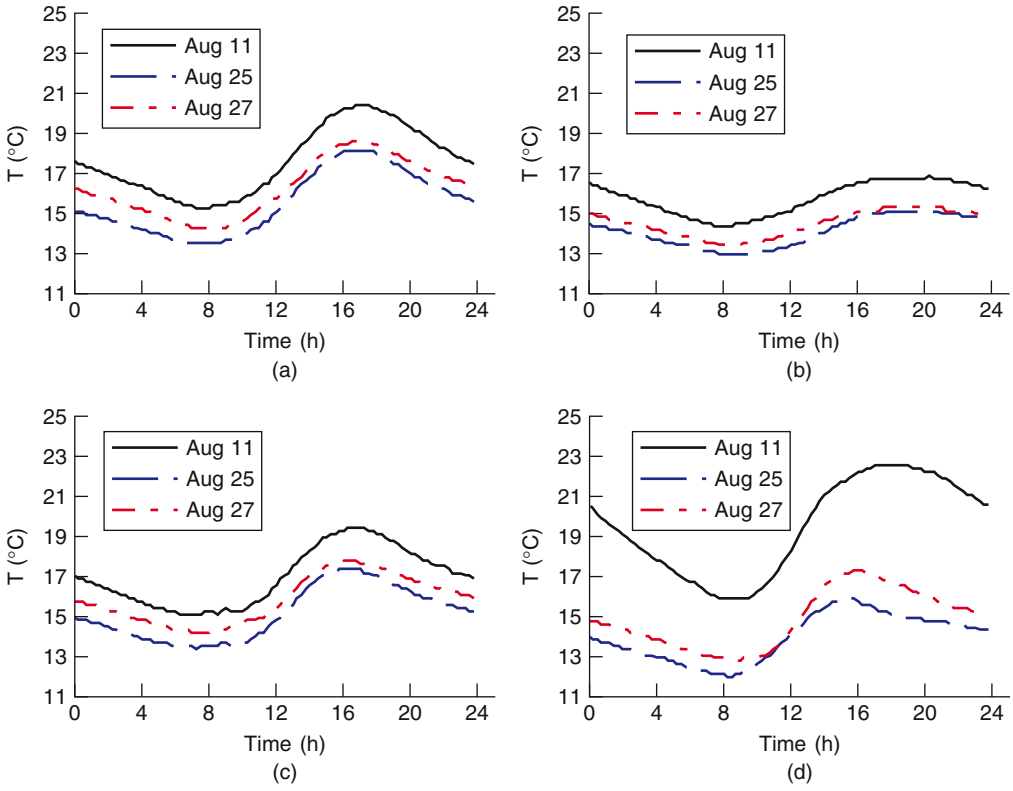

Figure 5.9 Change in temperature over time over a day for four locations: (a) a large river with an open riparian zone, (b) a small stream with an open riparian zone, (c) a large river with forested riparian zone, and (d) a small stream with forested riparian zone.

should not vary by more than $\pm 1\,^{\circ}$C from the TIR image, a window of more than 4 hr is possible, but to constrain measurements to within $\pm 0.5\,^{\circ}$C a window of less than 2 hr may be better.

5.6.2 Sampling site selection

The number of sampling sites is dictated by the (1) length of river to be measured, (2) its accessibility, and (3) the location of temperature extremes within the river. River length to be measured will be controlled by the method used for TIR image collection. For example, a single TIR image frame collected from a bridge, helicopter, or balloon may simply require field technicians to walk the length of the river reach, collecting representative temperature measurements. However, multiple aircraft images or even a single satellite image may cover 10s to 100s of kilometers of river channel, requiring in-stream sampling at many locations with multiple field teams. If recent TIR images are available, they can be used to select validation sites, and hand-held TIR sensors can be used to survey a region to determine optimum locations for deploying thermometers for longer-term monitoring.

Where digital spatial datasets of roads and river channels are available, an initial set of sampling locations can be devised by identifying locations where rivers and roads cross or come very close to each other. Otherwise local maps can be used for a similar search. In some cases it may be possible to determine if sites are inaccessible from available maps, air photos, and other spatial data layers within a GIS or Google Earth (Google Inc., 2010). For example, such data sources can be used to identify the presence of restricted lands, steep slopes, or channels that are not visible from above through dense riparian canopies. However, in many cases determining accessibility will require a survey of the locations to avoid inappropriate sample sites.

When identifying sampling locations, care should be taken to avoid locally cool or warm locations. These can be caused by the influence of tributaries, back-water

effects (where a dam or other obstruction results in changed temperature upstream), and groundwater seeps, which can change the bulk T_k of the main river channel locally. Fine-scale examples can be seen in Figures 5.1–5.3 in which seeps, springs, and tributaries affect water temperature at spatial scales of a few to 100s of m. The mixing of two very large tributaries, such as the Mississippi and Ohio rivers (USA) (Figure 5.7) can affect water temperature for many kilometers. In measurements made on the Columbia River (USA) using a hand-held thermometer, thermal eddies were revealed at the edge of the wide river, suggesting that more frequent measurements ($\sim$1 min^{-1}) might be necessary when the river is not well-mixed or in the presence of obstructions (Handcock et al., 2006).

5.6.3 Thermal stratification and mixing

As suggested by Wunderlich (1969), the effects of thermal stratification on data collection can be minimised by collecting measurements in shallow, well-mixed parts of the river because sites that are exposed to solar radiation, slow moving currents, or substantial cold-water inflows from seeps or springs may experience substantial thermal stratification (Nielson et al., 1994; Matthews and Berg, 1997; Torgersen et al., 2001). Thermal stratification is possible during sunny conditions or slow river flows when solar heating of the surface layer is not compensated by vertical mixing. For example, thermal stratification was observed by Torgersen et al. (2001) in some areas of the river that were not well mixed. Nielsen et al. (1994) found significant vertical stratification for flows of less than 1 ms^{-2} in the Middle Fork Eel River in northern California. They found that at depth, water could be as much as 7 °C cooler than at the surface. These examples highlight that TIR images only measure the water's surface, and that there are complex mixing processes deeper in the water column. For a good discussion of this issue and the physics of mixing, see Torgersen et al. (2001).

Wind and the breaking of waves can also disturb the skin layer and leave the surface well mixed, as has been seen in studies of ocean waves (Jessup et al., 1997), so that the measured T_r approaches the T_k of the water at the depth of mixing. Hook et al. (2003) investigated the difference between T_k in the surface layer and the T_r in the skin layer of lakes using four monitoring stations permanently moored on Lake Tahoe, California–Nevada (USA). They found a difference between T_k and T_r that varied over the diurnal cycle, which they attributed to solar heating and lower wind speeds in the morning. Water in rivers is more turbulent than in lakes and oceans, so beyond the potential for wind mixing, river flow around and over rocks, woody debris and other obstructions induces additional mixing and will break the skin layer. Because of this additional mixing, temperature derived from TIR images for turbulent rivers should be more representative of T_k than data for more static circumstances.

5.6.4 Measuring representative temperature

The use of hand-held, ground-based TIR thermometers, or small imaging radiometers, provides the most direct validation of remotely determined temperature. However, obtaining accurate temperature from such devices can be difficult. Because TIR radiation is emitted by all objects at all temperatures, the potential for contamination of readings from a radiant thermometer is high. Contact sensors, which include analog and digital sensors, are more robust and accurate, but they measure T_k at depth, thereby reducing their utility for comparison with T_r. T_k is the environmentally and ecologically important temperature but is not a direct comparison with what the remote TIR sensor detects. For example, in oceanographic applications where SST is of interest, a regression is usually applied between *in situ* T_k measured from buoys and ships and T_r from TIR sensors (Robinson et al., 1984) to convert the skin temperature measurement of T_k into T_k from deeper in the water column.

This regression approach is especially important for SST measurements since bulk T_k measurements have traditionally been collected at depths of up to 1 m. Such measurements can lead to values of T_k that are 0.1 to 1.5 K warmer than near-surface measurements of T_k. Capturing representative river temperature is potentially more difficult than in the ocean as water depths can change, there can be exchanges of water between the water and the streambed, and there can be spatial variability of temperature along and across the channel. For that reason, the collection of representative temperature of streams and rivers must be handled with care, both for ground-truth evaluation of remote sensing products and for capturing the ecologically sensitive values of T_k.

Precision of thermometers should be at least as good as that expected from the TIR measurements. For example, if the TIR sensor provides temperature with an NEΔT of 0.5 °C, a bulb thermometer should have lines at least every 1.0 °C so that temperature can be measured and recorded with a precision of 0.5 °C.

5.6.4.1 Radiant temperature measurement

There are many types of TIR thermometers available on the market ranging from under $100 to several thousand dollars (USA). These thermometers use similar technology to the satellite- and aircraft-based TIR imaging sensors, to detect the radiation emitted in the TIR spectrum; however, they are typically designed to measure the temperature of a single location, not to provide spatially extensive images, and are sensitive to the entire TIR spectral range rather than a narrow spectral range. Increased price for TIR imaging sensors will generally provide better optics, aiming capabilities and insulation. The latter is important for obtaining accurate temperature, as it reduces the sensitivity of the device to environmental conditions such as rapid heating or cooling of the internal components of the thermometer, which will change the amount of unintended TIR radiation reaching the sensor. Experiments with an inexpensive TIR thermometer (e.g., a TempTestr-IR from Oakton, 2005) showed that even short-term exposure to direct solar radiation in a climate-controlled building could substantially alter temperature readings from the thermometer (by several degrees Celsius). Increasing the insulation around the TIR thermometer and limiting its direct exposure to extreme conditions (such as direct solar radiation) can reduce the uncertainty in the measurement.

Care must also be taken that the TIR radiant thermometer is measuring only water temperature. These devices have a distance to target/spot size ratio that will indicate how wide the area being sensed is at different distances from target. Inexpensive sensors will typically have a lower ratio (e.g., 6:1, or 9.5°), in which case the spot diameter increases by 1 cm for every 6 cm greater distance of the target. The target area for less expensive devices will expand more rapidly with distance than for a more expensive device (e.g., with a ratio of 75:1, or 0.76°). The ratio should be smaller if measurements are made closer to the target in order to reduce the likelihood of interfering objects (e.g., rocks, logs) being included in the measurement.

These TIR radiant thermometers require that a single representative ε be specified, to ensure that the output temperature is appropriate for the material being measured. Higher temperature accuracy can be obtained by using accurate emissivities, but for spectrally variable targets, an accuracy limit is reached because the target is a selective radiator and not, in fact, a graybody. For example, for distilled water at 300 K the emissivities between 10 and 14μm range from 0.965 to 0.993, but using a single average emissivity of 0.985 will result in calculated temperatures of 29.00–28.69 °C (~0.3 K error). Ultimately, the change in temperature resulting from the emissivity correction is likely to be small relative to the other sources of error when using inexpensive devices.

5.6.4.2 Kinetic temperature measurement

There are a variety of technologies used for the measurement of T_k. These can be divided into analog and digital technologies and hand-held and self-contained temperature-logging units. Analog thermometers, most notably bulb thermometers, have traditionally been less expensive and therefore easier to supply to many field staff taking measurements. Digital thermometers may be easier to read and are potentially more robust. Self-contained data loggers are still the most expensive option, but they can be used to monitor water temperature for extended periods of time and in locations where regular access may be difficult. A combination of devices can provide an expanded network of observations in conjunction with an image acquisition as long as all devices are calibrated and care is taken in selecting measurement locations.

Thermometers will generally be used to measure water temperature near the water surface since the measured temperature will need to be read from the device and recorded. Because inserting the thermometer into the water will break any skin layer, such measurements will always be of the bulk water, not the skin itself. Measurements in the top 10 cm of water are most appropriate for comparison with calibrated TIR images, although the collection of simultaneous measurements can be difficult due to personnel restrictions. Temperature measured by data loggers mounted to the streambed tends to be lower than that measured using near-surface thermometers and TIR sensors. As with measurements of SST, this temperature difference is likely the result of thermal stratification (see Section 5.6.3 for more details).

In the next sections, we apply the knowledge described in this theoretical background to two examples of using TIR remote sensing to monitor water temperature.

5.6.5 Key points

- When absolute water temperature is required, it is necessary to collect validation data. If only relative temperature differences are required, validation data requirements can be reduced or eliminated.

- The number of sampling sites is dictated by the (1) length of river to be measured, (2) its accessibility, and (3) the location of temperature extremes within the river. Care should be taken to avoid locally cool or warm locations, as validation is best made where temperatures represent the bulk of the region being observed.
- Validation data can be collected from automatic gauges, or from surveys with radiant or kinetic thermometers with or without a data logger. A combination of devices can provide an expanded network of observations in conjunction with an image acquisition as long as all devices are calibrated and care is taken in selecting measurement locations.
  - Measurements using hand-held kinetic thermometers to measure T_k (i.e., analog, digital, or data logger) will generally be near the water surface, and because inserting the thermometer into the water will break any skin layer, such measurements will always be of the bulk water, not the skin itself.
  - Analog thermometers are usually less expensive, but digital thermometers may be easier to read and are potentially more robust. Both can be used to rapidly expand a sampling network with trained volunteers for a single day of observations.
  - Self-contained data loggers are the most expensive option, but they can be used to monitor water temperature deeper in the water column, for extended periods of time, and in locations where regular access may be difficult.
  - Radiant thermometers can be used to survey a region for appropriate sampling locations. They are, however, generally sensitive to the entire TIR spectral range, and require that a single representative ε be specified. Such thermometers are also generally sensitive to their own temperature so care should be taken when using them in the field.
- Measured T_r represents the 'skin' layer at the water surface. Depending on the amount of mixing in the river, it may not be representative of T_k further down in the water column.
- The effects of thermal stratification on data collection can be minimised by collecting measurements in shallow, well-mixed parts of the river because sites that are exposed to solar radiation, slow moving currents, or substantial cold-water inflows from seeps or springs may experience substantial thermal stratification.
- Water temperature should be measured close enough to the time of the TIR image collection that the temperature has not changed significantly (see Section 5.6.1).
- Precision of thermometers should be at least as good as that expected from the TIR measurements.

5.7 Example 1: Illustrating the necessity of matching the spatial resolution of the TIR imaging device to river width using multi-scale observations of water temperature in the Pacific Northwest (USA)

In this section, we show examples of TIR remote sensing of water across a range of stream widths and pixel sizes, to illustrate the necessity of matching the specifications of the TIR imaging sensor to the river characteristics such as the channel width. The combination of the spatial resolution of TIR images and river width both affect the accuracy and uncertainty of recovered in-stream T_r (Handcock et al., 2006). The accuracy is of great importance in that any detectable spatial pattern in temperature could be evidence for identifying thermal features such as springs, seeping cold water or subsurface flow. To illustrate the consistency between T_r and T_k fully, longitudinal profiles of radiant temperature from downstream to headwater stream reaches can be plotted in order to compare with the *in situ* gage observations. The mean difference and the standard error (deviation) of temperature are important metrics for evaluating the accuracy of temperature extraction.

As an example of these concepts, we have provided a group of images for reaches of the Green River, Washington (USA), as remotely sensed from TIR imaging sensors with pixel sizes of 5 m (MASTER), 15 m (MASTER), 60 m (Landsat 7 ETM^+) and 90 m (ASTER) respectively (Figure 5.10a). Although Green River was clearly visible under MASTER and Landsat sensors, this river reach was obscured in the 90 m pixel size of the ASTER image. In our analysis, data were extracted along centre-lines of the river, in order to remove geo-referencing errors and possible along-stream mixed pixels. The results showed that in the 5 m MASTER image, the Green River along-stream radiant temperature had a standard deviation of 0.7 °C and the mean difference between radiant temperature and kinetic temperature was +1.9 °C. The fact that the 0.7 °C variability was close to the NEΔT for the MASTER sensor (0.46–0.71 °C; Hook et al., 2001) indicated no obvious influence from warmer bank temperature. In contrast, the standard deviation was 1.6 °C and the mean difference was +2.1 °C for the 15 m pixels

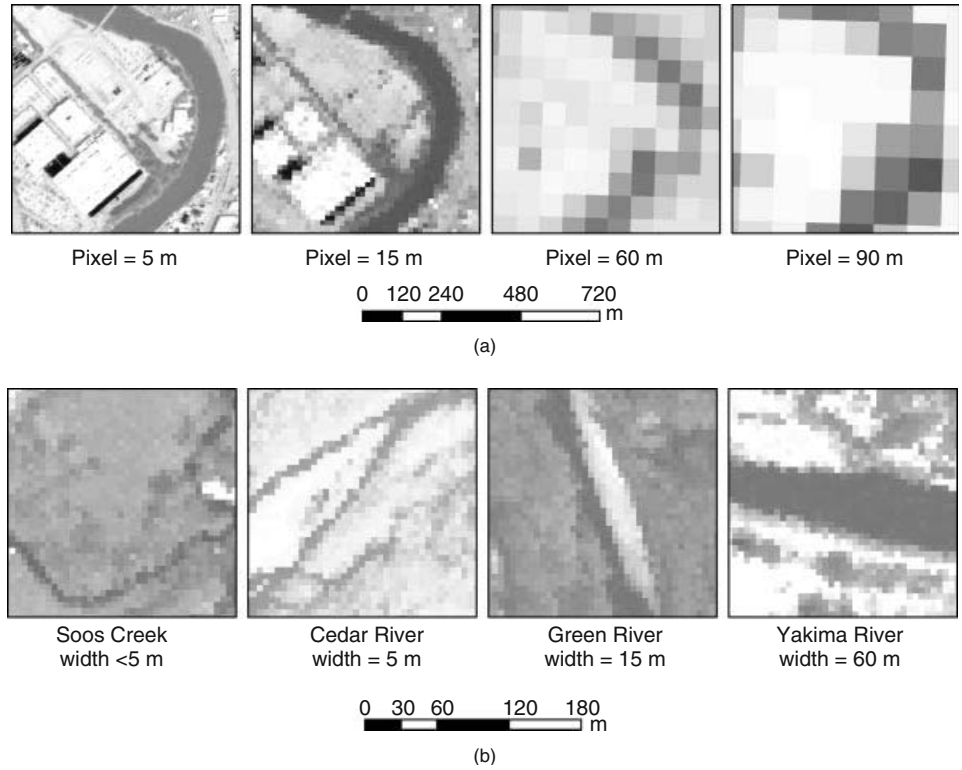

Figure 5.10 Examples of 1 km^2 TIR image subsets (a) from different TIR sensors for a single location on the Green River Washington (USA) at different pixel sizes to illustrate the effect of pixel size on what can be seen, and (b) with a set 5 m pixel size from the MASTER sensor for a range of stream widths from streams in Washington (USA) observed at different pixel sizes to show the interaction between stream width and pixel size. For these un-calibrated images, darker shades indicate lower temperatures, and lighter shades higher temperatures.

of the MASTER data. This increased variability can be explained by the effects from warmer bank temperature because the along-stream temperature variability pattern was still similar to that of the 5 m MASTER image in some locations. In comparison, for the 90 m ASTER image, the mean difference increased to 4.6 °C, with the standard deviation decreasing to 4.6 °C, which is much larger than the NEΔT of ASTER sensor ($\leq$0.3 °C at 27 °C; Gillespie et al., 1998; Yamaguchi et al., 1998). Consequently, the Green River was fully resolved by the 5 m pixel size of the MASTER sensor, partly resolved by the 15 m pixels of the MASTER, and not resolved by the 90 m pixels of the ASTER sensor to obtain radiant temperature. See Cherkauer et al. (2005) for a detailed description and discussion.

A similar problem can be illustrated by evaluating different width reaches at a single TIR imaging sensor resolution, such as the 5 m resolution MASTER images used in Figure 5.10b. Here, Soos Creek with a width of less than 5 m, had mixed at the bank, and the water was never fully resolved. Water pixels could occasionally be fully resolved in the Cedar River whose average width was equivalent to the resolution of the TIR image of about 5 m, whereas determining water temperature was easier for both the Green River with widths equal to approximately three pixels, and the Yakima River with greater than three pixels. As described previously, narrow stream widths will result in the problem of mixed pixels along the stream. Generally, at least three pure-water pixels are needed in order for an accurate temperature extraction (assuming that there are no sub-pixel obstructions within the stream), and as the number of pixels across the stream decreases, the accuracies decrease and uncertainties increase (Handcock et al., 2006).

5.8 Example 2: Thermal heterogeneity in river floodplains used to assess habitat diversity

In this example, we expand our scope from looking at water in narrow stream and river reaches using multi-scale data, to show an example of thermal heterogeneity in the river floodplain as an indicator of habitat diversity. River floodplains are transitional areas that extend from the edge of permanent water bodies to the edge of uplands. In their natural state, they are among the most complex, dynamic, and diverse ecosystems globally, characterised by interacting flow, thermal, and sediment pulses that provide a complex 'template' to which organisms are adapted and by which ecosystem processes are controlled (Naiman et al., 2005; Stanford et al., 2005; Tockner et al., 2010). Although the changes in the composition and the configuration of habitat types have been well documented, little is known about thermal patch dynamics at the landscape scale (cf. Cardenas et al., 2008; Smikrud et al., 2008). Thermal patch dynamics are expected to control the distribution of aquatic and terrestrial organisms as well as of animals that exhibit complex life cycles (e.g., aquatic insects, amphibians). Furthermore, information on thermal heterogeneity is required to 'scale-up' ecosystem processes from the patch to the entire ecosystem.

In a recent study, Tonolla et al. (2010) applied ground-based TIR images to quantify surface temperature patterns at 12–15 minute intervals over 24 h cycles in near-natural Alpine river floodplains (Roseg, Tagliamento River; Figure 5.11). Each habitat type exhibited a distinct thermal signature creating a complex thermal mosaic. The diel temperature pulse and maximum daily temperature were the main thermal components that differentiated the various aquatic and terrestrial habitat types. In both river floodplains, exposed gravel sediments exhibited the highest diel pulse (up to 23 °C) while in aquatic habitats the pulse was as low as 11 °C. At the floodplain scale, thermal heterogeneity was low during night-time but strongly increased during day time, thereby creating a complex shifting mosaic of thermal patches (Figure 5.11). However, TIR images only record T_r at the water surface. Within the top 29 cm of the unsaturated gravel sediments, thermal heterogeneity was as high as across the entire floodplain at the surface (Tonolla et al., 2010). This strong vertical gradient should be considered when calculating temperature-dependent ecosystem processes.

This study emphasised that remotely sensed TIR images provide a unique opportunity to simultaneously map surface temperature of aquatic and terrestrial ecosystems at a high spatio-temporal resolution, a capability not possible using non-imaging ground-based methods (e.g., Arscott et al., 2001; Kaushal et al., 2010). However, a major challenge is to link thermal patch dynamics with ecological processes. Indermaur et al. (2009a, b), for example, demonstrated that home range placement of amphibians in the Tagliamento floodplain depends on the thermal properties of the individual habitat types (e.g., large wood deposits that provide thermal refugia), as well as on the spatial configuration of these habitats. Furthermore, there is clear evidence that the diel temperature pulses are ecologically more relevant than the average daily temperature. Microbial activity, for example, immediately reacts to short-term alterations in temperature leading to rapid alterations in ecosystem respiration when temperature changes. Therefore, ignoring local-scale and short-term thermal dynamics may lead to false conclusions about environmental change impacts on ecosystems. Concurrently, the effects of global warming can be attenuated by manipulating specific habitat characteristics and processes such as vegetation cover and the exchange between subsurface and surface water.

The use of airborne vehicles mounted with TIR imaging sensors can be extended to map the riparian areas, for example, mapping floodplains at different flow conditions and studying the distribution and density of terrestrial mammals such as deer or wild boar during flood events (e.g., Naugle et al., 1996). Furthermore, the TIR technique can be used in combination with other sensors such as LIDAR to quantify the three-dimensional heterogeneity of river floodplains.

5.9 Summary

In this chapter, we showed how TIR measurements can be used for observing water temperature in riverine landscapes for practical applications. We explored the theoretical basis of TIR observations of water temperature, data sources, the processing steps necessary to obtain accurate estimates of temperature in riverine environments from TIR data, and the validation of such temperature estimates. We also provided some multi-scale examples of the application of TIR data in riverine ecology and management. At the end of each section, and in Table 5.1, we have summarised some of the key points for managers using TIR data to monitor water temperature of stream and rivers. We hope that the

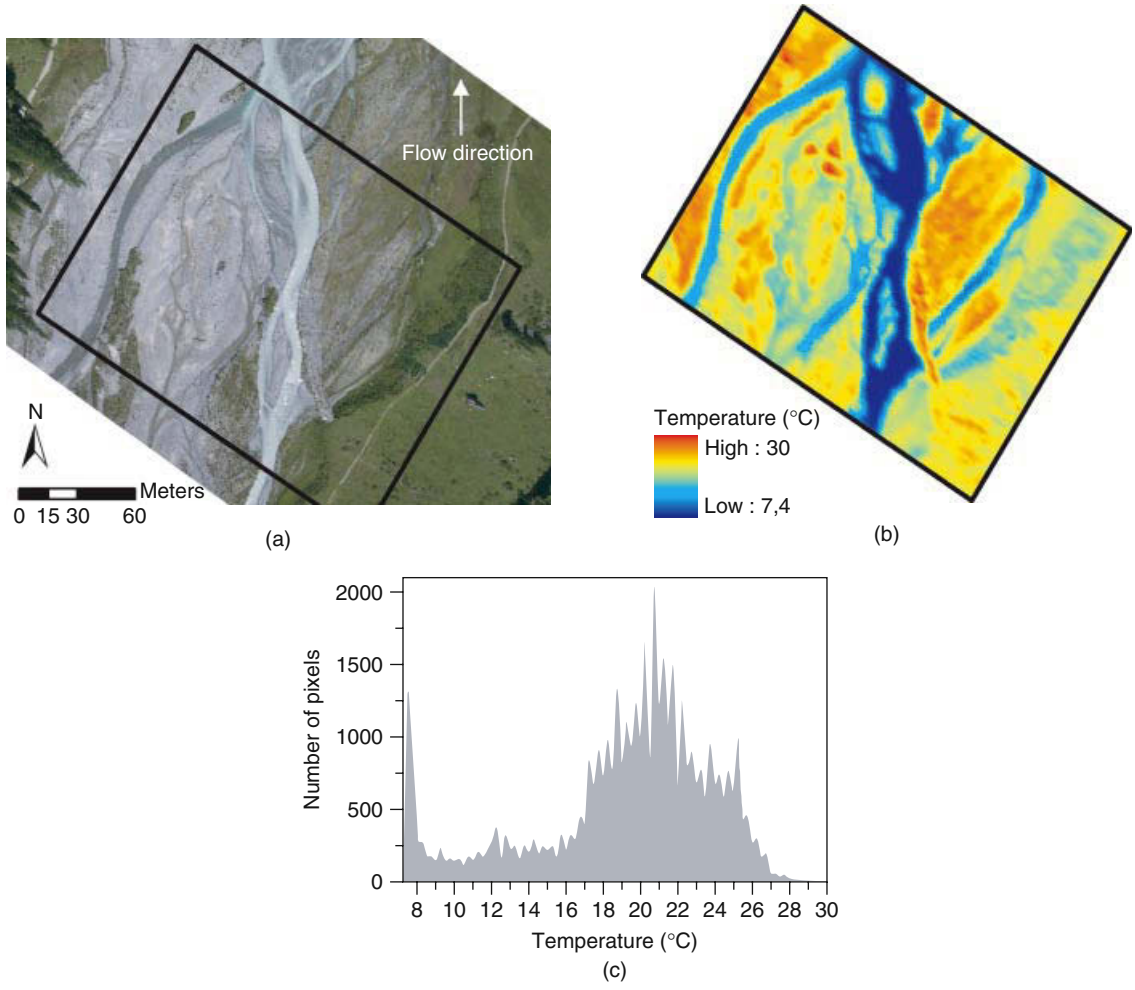

Figure 5.11 Geo-referenced natural-color image of the Roseg floodplain (a), airborne TIR image (b), and (c) frequency distribution radiant temperatures in TIR image (°C) at 15:00 (23 August 2004) (D. Tonolla, personal communication).

practical approach we took will be useful for the application of TIR remote sensing and can be successfully used in thermal monitoring of riverine landscapes.

Acknowledgements

Although the research described in the article has been funded in part by the United States Environmental Protection Agency's STAR program through grant R827675-01-0, it has not been subjected to EPA review, and does not necessarily reflect the views of the Agency, and no official endorsement should be inferred. Emissivity data reproduced from the MODIS Emissivity Library. This data set was collected by Dr. Zhengming Wan's Group at ICESS (Institute for Computational Earth System Science) located on the campus of UCSB (University of California, Santa Barbara). Any use of trade, product, or firm names is for descriptive purposes only and does not imply endorsement by the United States Government. We acknowledge the extensive contributions of M. Boyd (formerly with the Oregon Department of Environmental Quality, Portland, Oregon (USA), and currently with Watershed Sciences, Inc., Portland, Oregon, USA) for his development of river-temperature modeling techniques that utilised airborne TIR images for calibration and

led to airborne TIR data collection throughout thousands of kilometers of rivers and streams in Oregon and the Pacific Northwest (USA). We also thank Diego Tonolla, and H. Piegay and two anonymous reviewers for constructive comments.

5.10 Table of abbreviations

ASTER	NASA EOS Advanced Spaceborne Thermal Emission and Reflection radiometer
DN	Digital Number
ε	Emissivity
EPA	The United States Environmental Protection Agency
FAA	Federal Aviation Administration (USA)
FOV	Field of view
FLIR	Forward looking infrared
GPS	Global positioning system
GSD	Ground sampling distance
IFOV	Instantaneous field of view
IMU	Inertial measurement unit
L_p	Atmospheric path spectral radiance
L_g	Spectral radiance emitted at the ground-surface
L_s	Spectral radiance measured at the sensor
Landsat ETM$^+$	Sensor on the Landsat-7 spacecraft
W	Spectral radiant emittance
MASTER	MODIS/ASTER airborne simulator
MODIS	NASA EOS sensor on the Terra and Aqua spacecrafts
NEΔT	Noise-equivalent temperature change
NIR	Near infrared part of the electromagnetic spectrum
ρ	Reflectivity
SST	Sea-surface temperature
SWIR	Shortwave Infrared
τ	Atmospheric transmissivity
T_k	Kinetic water temperature
T_r	Radiant water temperature
TIR	Thermal Infrared
TOA	Top of atmosphere
UAV	Unmanned Aerial Vehicle
VNIR	Visible and near infrared parts of the electromagnetic spectrum
λ	Wavelength

References

Adler-Golden, S.M., Matthew, M.W., Bernstein, L.S., Levine, R.Y., Berk, A., Richtsmeier, S.C., Acharya, P.K., Anderson, G.P., Felde, G., Gardner, J., Hike, M., Jeong, L.S., Pukall, B., Mello, J., Ratkowski, A., and Burke, H.-H. (1999). Atmospheric correction for shortwave spectral imagery based on MODTRAN4. *SPIE Proc. Imaging Spectrometry*, 3753, 61–69.

Anding, D. and Kauth, R. (1970). Estimation of Sea Surface Temperature from space. *Remote Sensing of Environment*, 1, 217–220.

Arrigoni, A.S., Poole, G.C., Mertes, L.A.K., O'Daniel, S.J., Woessner, W.W., and Thomas, S.A. (2008). Buffered, lagged, or cooled? Disentangling hyporheic influences on temperature cycles in stream channels. *Water Resources Research*, 44 (W09418).

Arscott, D.B., Tockner, K., and Ward, J.V. (2001). Thermal heterogeneity along a braided floodplain river (Tagliamento River, northeastern Italy). *Canadian Journal of Fisheries and Aquatic Sciences*, 58, 2359–2373.

Atwell, B.H., MacDonald, R.B., and Bartolucci, L.A. (1971). Thermal Mapping of Streams from airborne Radiometric Scanning. *Water Resources Bulletin*, 7 (2), 228–243.

Baird, O.E. and Krueger, C.C. (2003). Behavioral thermoregulation of brook and rainbow trout: Comparison of summer habitat use in an Adirondack River, New York. *Transactions of the American Fisheries Society*, 132, 1194–1206.

Baldridge, A.M., Hook, S.J., Grove, C.I., and G. Rivera, G. (2009). The ASTER Spectral Library Version 2.0. *Remote Sensing of Environment*, 113 (4), 711–715.

Barnes, W.L., Pagano, T.S., and Salomonson, V.V. (1998). Prelaunch characteristics of the Moderate Resolution Imaging Spectroradiometer (MODIS) on EOS-AM1. *IEEE Transactions on Geoscience and Remote Sensing*, 36 (4), 1088–1100.

Bartholomew, M.J., Kahle, A.B., and Hoover, G. (1989). Infrared spectroscopy (2, 3-20 μm) for the geological interpretation of remotely-sensed multispectral thermal infrared data. *International Journal of Remote Sensing*, 10 (3), 529–544.

Belknap, W. and Naiman, R.J. (1998). A GIS and TIR procedure to detect and map wall-base channels in western Washington. *Journal of Environmental Management*, 52, 147–160.

Berk, A., Bernstein, L.S., and Robertson, D.C. (1989). MODTRAN: a moderate resolution model for LOWTRAN7. GL-TR-90-0122. Technical Report. Geophysics Directorate, Phillips Laboratory, Hanscom, AFB, MA. 44 pp.

Berni, J.A.J., Zarco-Tejada, P.J., Suarez, L., Fereres, and E. (2009). Thermal and Narrow-band Multispectral Remote Sensing for Vegetation Monitoring from an Unmanned Aerial Vehicle. *IEEE Transactions on Geoscience and Remote Sensing*, 47, 722–738.

Beschta, R.L., Bilby, R.E., Brown, G.W., Holtby, L.B., and Hofstra, T.D. (1987). Stream temperature and aquatic habitat: Fisheries and forestry interactions. In Streamside management: Forestry and fishery interactions. Salo, E.O. and Cundy,

T.W. (eds). University of Washington, Institute of Forest Resources: Seattle, USA: 191–232.

Bolgrien, D.W. and Brooks, A.S. (1992). Analysis of thermal features of Lake-Michigan from AVHRR satellite images. *Journal of Great Lakes Research*, 18 (2), 259–266.

Boyd, M. and Kasper, B. (2003). Analytical methods for dynamic open channel heat and mass transfer: Methodology for Heat Source Model Version 7.0. http://www.deq.state.or.us/wq/TMDLs/tools.htm (Last accessed 25th July 2010)

Brown, G.W. and Krieger, J.T. (1970). Effects of clear-cutting on stream temperature. *Water Resources Research*, 6 (4), 1133–1139.

Burkholder, B.K., Grant, G.E., Haggerty, R., Khangaonkar, T., and Wampler, P.J. (2008). Influence of hyporheic flow and geomorphology on temperature of a large, gravel-bed river, Clackamas River, Oregon. *Hydrological Processes*, 22, 941–953.

Cardenas, M.B., Harvey, J.W., Packman, A.I., and Scott, D.T. (2008). Ground-based thermography of fluvial systems at low and high discharge reveals complex thermal heterogeneity driven by flow variation and bioroughness. *Hydrological Processes*, 22, 980–986.

Cardenas, M.B., Neale, C.M.U., Jaworowski, C., and Heasler, H. (2011). High-resolution mapping of river-hydrothermal water mixing: Yellowstone National Park. *International Journal of Remote Sensing*, 32, 2765–2777.

Chen, Y.D., Carsel, R.F., McCutcheon, S.C., and Nutter, W.L. (1998). Stream temperature simulation of forested riparian areas: I. watershed-scale model development. *Journal of Environmental Engineering*, 124 (4), 304–315.

Chen, C.Q., Shi, P., and Mao, Q.W. (2003). Application of remote sensing techniques for monitoring the thermal pollution of cooling-water discharge from nuclear power plant. *Journal of Environmental Science and Health Part A*, 38 (8), 1659–1668.

Cherkauer, K.A., Burges, S.J., Handcock, R.N., Kay, J.E., Kampf, S.K., and Gillespie, A.R. (2005). Assessing satellite-based thermal-infrared remote-sensing for monitoring Pacific Northwest river temperatures. *Journal of the American Water Resources Association*, October. Paper No. 03161.

Cristea, N.C. and Burges, S.J. (2009). Use of Thermal Infrared Imagery to Complement Monitoring and Modeling of Spatial Stream Temperatures. *Journal of Hydrologic Engineering*, Oct 2009, 1080:1090.

Cuenca, J. and Sobrino, J.A. (2004). Experimental measurements for studying angular and spectral variation of thermal infrared emissivity. *Applied Optics*, 43 (23), 4598–4602.

de Jong, S.M., and van der Meer, F.D. (Eds.) (2004). Remote sensing image analysis: including the spatial domain, Dordrecht: London, p. 359.

Dahle, S. (2009). Predicting the growth potential of a shallow, warm-water sport fishery: A spatially explicit bioenergetics approach. MSc Thesis, Utah State University, pp. 49.

Danielescu, S., MacQuarrie, K.T.B., and Faux, R.N. (2009). The integration of thermal infrared imaging, discharge measurements and numerical simulation to quantify the relative contributions of freshwater inflows to small estuaries in Atlantic Canada. *Hydrological Processes*, 23 (20), 2847–2859.

Dudhia, J. (1993). A non-hydrostatic version of the Penn State-NCAR mesoscale model: validation tests and simulation of an Atlantic cyclone and cold front. *Monthly Weather Review*, 121, 1493–1513.

Dunckel, A.E., Cardenas, M.B., Sawyer, A.H., and Bennett, P.C. (2009). High-resolution in-situ thermal imaging of microbial mats at El Tatio Geyser, Chile shows coupling between community color and temperature. *Geophysical Research Letters*, 36 (L23403), 5 pp, doi:10.1029/2009GL041366.

Ebersole, J.L., Liss, W.J., and Frissell, C.A. (2001). Relationship between stream temperature, thermal refugia and rainbow trout Oncorhynchus mykiss abundance in arid-land streams in the northwestern United States. *Ecology of Freshwater Fish*, 10, 1–10.

Emery, W.J. and Yu Y. (1997). Satellite sea surface temperature patterns. *International Journal of Remote Sensing*, 18 (2), 323–334.

Environmental Protection Agency (2003). EPA Region 10 guidance for Pacific Northwest state and tribal temperature water quality standards. Region 10 Office of Water, Seattle, WA. EPA 910-B-03-002. 57 pp.

Faux, R.N. and McIntosh, B.A. (2000). Stream temperature assessment. *Conservation in Practice*, 1, 38–39.

Faux, R.N., Lachowsky, H., Maus, P., Torgersen, C.E., and Boyd, M.S. (2001). New approaches for monitoring stream temperature: Airborne thermal infrared remote sensing. Remote Sensing Applications Laboratory, USDA Forest Service, Salt Lake City, Utah.

Gillespie, A.R. (1992). Spectral mixture analysis of multispectral thermal infrared images. *Remote Sensing of Environment*, 42, 137–145.

Gillespie, A.R., Kahle, A.B., and Palluconi, F.D. (1984). Mapping alluvial fans in Death Valley, California, using multichannel thermal infrared images. *Geophysical. Research. Letters*, 11 (11), 1153–1156.

Gillespie, A.R., Rokugawa, S., Matsunaga, T., Cothern, J.S., Hook, S., and Kahle, A.B. (1998). A temperature and emissivity separation algorithm for ASTER images. *IEEE Transactions on Geoscience and Remote Sensing*, 36 (4), 1113–1126.

Google Inc. (2010). Google Earth (Version 5.0), http://www.google.com/earth/index.html (Last accessed 25th July 2010).

Gu, Y., Zhang, Y., and Zhang, J. (2008). Integration of spatial-spectral information for resolution enhancement in hyperspectral images. IEEE *Transactions on Geoscience and Remote Sensing*, 46 (5), 1347–1358. DOI: 10.1109/TGRS.2008.917270.

Gustafson, W.T., Handcock, R.N., Gillespie, A.R., and Tonooka, H. (2003). Image sharpening method to recover stream temperatures from ASTER images. Proceedings SPIE International Society for Optical Engineering. *Remote Sensing for Environmental Monitoring*, 4886 (72).

Handcock, R.N., Cherkauer, K.A., Kay, J.E., Gillespie, A., Burges, S.J., and Booth, D.B. (2002). Spatial Variability in Radiant Stream Temperatures Estimated from Thermal Infrared Images. *Eos Transactions AGU*, 83 (47), Fall Meet. Suppl., Abstract H72 E-0896, 2002.

Handcock, R.N., Gillespie, A., Cherkauer, K.A., Kay, J.E., Burges, S.J., and Kampf, S.K. (2006). Accuracy and uncertainty of thermal-infrared remote sensing of stream temperatures at multiple spatial scales. *Remote Sensing of Environment*, 100, 427–440.

Hick, P.T., and Carlton, M.D.W. (1991). Practical applications of airborne multispectral scanner data for forest, agriculture, and environmental monitoring. Pages 60–61 in 24th International Symposium on Remote Sensing of Environment, Rio de Janeiro, Brazil.

High, B., Peery, C.A., and Bennett, D.H. (2006). Temporary staging of Columbia River summer steelhead in coolwater areas and its effect on migration rates. *Transactions of the American Fisheries Society*, 135, 519–528.

Hook, S.J., Myers, J.J., Thome, K.J., Fitzgerald, M., and Kahle, A.B. (2001). The MODIS/ASTER airborne simulator (MASTER) – a new instrument for earth science studies. *Remote Sensing of Environment*, 76 (1), 93–102.

Hook, S.J., Prata, F.J., Alley, R.E., Abtahi, A., Richards, R.C., Schladow, S.G., and Palmarsson, S.O. (2003). Retrieval of lake bulk and skin temperatures using Along-Track Scanning Radiometer (ATSR-2) data: A case study using Lake Tahoe, California. *Journal of Atmospheric and Oceanic Technology*, 20 (4), 534–548.

Indermaur, L., Gehring, M., Wehrle, W., Tockner, K., and Näf-Dänzer, B. (2009a). Behavior-based scale definitions for determining individual space use: requirement of two amphibians. *The American Naturalist*, 173, 60–71.

Indermaur, L., Winzeler, T., Schmidt, B.R., Tockner, K., and Schaub, M. (2009b). Differential resource selection within shared habitat types across spatial scales in sympatric toads. *Ecology*, 90, 3430–3444.

Ishiyama, T., Tsuchiya, K., and Sugihara, S. (1995). Influence of look-angle on the water-surface temperature observed with an IR radiometer, *Advances in Space Research*, 17 (1), 43–46.

Jessup, A.T., Zappa, C.J., Loewen, M.R., and Hesany, V. (1997). Infrared remote sensing of breaking waves. *Nature*, 385 (6611), 52–55.

Kay, J.E., Kampf, S.K., Handcock, R., Cherkauer, K., Gillespie, A.R., and Burges, S.J. (2005). Accuracy of lake and stream temperatures estimated from thermal infrared imagery. *Journal of the American Water Resources Association*, October. Paper No. 04102.

Kahle, A.B., Palluconi, F.D., Hook, S.J., Realmuto, V.J., and Bothwell, G. (1991). The Advanced Spaceborne Thermal Emission and Reflectance Radiometer (ASTER). *International Journal of Imaging Systems Technology*, 3, 144–156.

Kaushal, S.S., Likens, G.E., Jaworski, N.A., Pace, M.L., Sides, A.M., Seekell, D., Belt, K.T., Secor, D.H., and Wingate, R.L. (2010). Rising stream and river temperatures in the United States. Frontiers in Ecology and the Environment (e-View). doi:10.1890/090037.

Kilpatrick, K.A., Podesta, G.P., and Evans, R. (2001). Overview of the NOAA/NASA advanced very high resolution radiometer Pathfinder algorithm for sea surface temperature and associated matchup database. *Journal of Geophysical Research-Oceans*, 106 (C5), 9179–9197.

Kotchenova, S.Y., Vermote, E.F., Matarrese, R., and Klemm, Jr., F.J. (2006). Validation of a vector version of the 6S radiative transfer code for atmospheric correction of satellite data. Part I: Path Radiance. *Applied Optics*, 45, 6762–6774.

LeDrew, E.F. and Franklin, S.E. (1985). The use of thermal infrared imagery in surface current analysis of a small lake. *Photogrammetric Engineering and Remote Sensing*, 51, 565–573.

Lillesand, T.M., Kiefer, R.W., and Chipman, J.W. (2008). Remote sensing and image interpretation, 6th Ed.; John Wiley and Sons: Hoboken, USA, p. 768.

Loheide, S.P. and Gorelick, S.M. (2006). Quantifying stream-aquifer interactions through the analysis of remotely sensed thermographic profiles and *in situ* temperature histories. *Environmental Science and Technology*, 40, 3336–3341.

Madej, M.A., Currens, C., Ozaki, V., Yee, J., and Anderson, D.G. (2006). Assessing possible thermal rearing restrictions for juvenile coho salmon (Oncorhynchus kisutch) through thermal infrared imaging and in-stream monitoring, Redwood Creek, California. *Canadian Journal of Fisheries and Aquatic Sciences*, 63, 1384–1396.

Masuda, K., Takashima, T., and Takayama, Y. (1988). Emissivity of pure and sea waters for the model sea-surface in the infrared window regions. *Remote Sensing of Environment*, 24 (2), 313–329.

Matthews, K.R. and Berg, N.H. (1997). Rainbow trout responses to water temperature and dissolved oxygen stress in two southern California stream pools. *Journal of Fish Biology*, 50 (1), 50–67.

Mather, P.M. (2004). Computer Processing of Remotely Sensed Images (3rd Ed.). John Wiley, Chichester, U.K.

McCullough, D.A., Bartholow, J.M., Jager, H.I., Beschta, R.L., Cheslak, E.F., Deas, M.L., Ebersole, J.L., Foott, J.S., Johnson, S.L., Marine, K.R., Mesa, M.G., Petersen, J.H., Souchon, Y., Tiffan, K.F., and Wurtsbaugh, W.A. (2009). Research in thermal biology: Burning questions for coldwater stream fishes. *Reviews in Fisheries Science*, 17, 90–115.

Mertes, L.A.K., Dekker, A.G., Brakenridge, G.R., Birkett, C.M., and Letourneau, G. (2004). Rivers and lakes. In Remote sensing for natural resource management and environmental monitoring. Manual of remote sensing. Volume 4, Ustin, S.L. (ed.) John Wiley & Sons, Inc.: Hoboken, New Jersey, pp. 345–400.

MODIS Emissivity Library. (2010). http://www.icess.ucsb.edu/modis/EMIS/html/em.html (Last accessed 25th July 2010).

Naiman, R.J., Decamps, H., and McClain, ME. (2005). Riparia. Elsevier/Academic Press. San Diego, USA.

National Aeronautics and Space Administration, (1998). Landsat-7 science data users handbook. Greenbelt, Maryland, NASA Goddard Space Flight Center, electronic version, http://landsathandbook.gsfc.nasa.gov/handbook/handbook_toc.html (Last accessed 25th July 2010).

Naugle, D.E., Jenks, J.A., and Kernohan B.J. (1996). Use of thermal infrared sensing to estimate density of white-tailed deer. *Wildlife Society Bulletin*, 24, 37–43.

Nielsen, J.L., Lisle, T.E., and Ozaki, V.L. (1994). Thermally stratified pools and their use by steelhead in northern California streams. *Transactions of the American Fisheries Society*, 123, 613–626.

Oakton (2005). http://www.4oakton.com/ (last accessed 25th July 2010).

Ontar Corporation (1998). PcModWin v 3.7, Village Way, North Andover, MA, 01845, USA.

Oregon Department of Environmental Quality (2006). Willamette Basin total maximum daily load (TMDL). Appendix C: Temperature. Oregon Department of Environmental Quality, Portland, OR, USA.

Oregon Department of Environmental Quality (2010a) http://www.deq.state.or.us/wq/tmdls/granderonde.htm (last accessed 25th July 2010).

Oregon Department of Environmental Quality (2010b) http://www.deq.state.or.us/wq/tmdls/docs/granderondebasin/upgronde/appxa.pdf (Last accessed 25th July 2010).

Parkinson, C.L. (2003). Aqua: An earth-observing satellite mission to examine water and other climate variables. *IEEE Transactions on Geoscience and Remote Sensing*, 41 (2), 173–183.

Poole, G.C. and Berman, C.H. (2001). An ecological perspective on in-stream temperature: Natural heat dynamics and mechanisms of human-caused thermal degradation. *Environmental Management*, 27, 787–802.

Prakash, A. (2000). Thermal remote sensing: Concepts, issues and applications. XIXth ISPRS Congress, July 16–23, Amsterdam, The Netherlands.

Rayne, S. and Henderson, G.S. (2004). Airborne thermal infrared remote sensing of stream and riparian temperatures in the Nicola River watershed, British Columbia, Canada. *Journal of Environmental Hydrology*, 14, 1–11.

Robinson, I.S., Wells, N.C., and Charnock, H. (1984). The sea surface thermal boundary layer and its relevance to the measurement of sea surface temperature by airborne and spaceborne radiometers. *International Journal of Remote Sensing*, 5, 19–45.

Roganalski, A. and Chrzanowski, K. (2002). Infrared devices and techniques. *Opto-Electronics Review*, 10 (2), 111–136.

Salisbury, J.W. and D'Aria, D.M. (1992). Emissivity of terrestrial materials in the 8-14 μm atmospheric window. *Remote Sensing of Environment*, 42, 83–106.

Sentlinger, G.I., Hook, S.J., and Laval, B. (2008). Sub-pixel water temperature estimation from thermal-infrared imagery using vectorized lake features. *Remote Sensing of Environment*, 112, 1678–1688.

Smikrud, K.M., Prakash, A., and Nicholos, J. (2008). Decision-based fusion for improved fluvial landscape classification using digital aerial photographs and forward looking infrared images. *Photogrammetric Engineering and Remote Sensing*, 74, 903–911.

Stanford, J.A., Lorang, M.S., and Hauer, F.R. (2005). The shifting habitat mosaic of river ecosystems. *Verhandlungen der Internationalen Vereinigung für Theoretische und Angewandte Limnologie*, 29, 123–136.

Tockner, K. (2006). Using ecological indicators to evaluate rehabilitation projects. EAWAG News 61e, Swiss Federal Institute for Environmental Science and Technology, Duebendorf, Switzerland.

Tockner, K., Lorang, M.S., and Stanford, J.A. (2010). River flood plains are model ecosystems to test general hydrogeomorphic and ecological concepts. *River Research and Applications*, 26, 76–86.

Torgersen, C.E., Price, D.M., Li, and H.W., and McIntosh, B.A. (1999). Multiscale thermal refugia and stream habitat associations of chinook salmon in northeastern Oregon. *Ecological Applications*, 9, 301–319.

Torgersen, C.E., Faux, R.N., McIntosh, B.A., Poage, N.J., and Norton, D.J. (2001). Airborne thermal remote sensing for water temperature assessment in rivers and streams. *Remote Sensing of Environment*, 76, 386–398.

Tonolla, D., Acuna, V., Uehlinger, U., Frank, T., and Tockner, K. (2010). Thermal heterogeneity in river floodplains. *Ecosystems*, 13, 727–740.

Washington Department of Ecology (1998). Washington State Water Quality Assessment Section, Report 305(b). Olympia, WA. 56 p.

Wunderlich, W O. (1969). The fully-mixed stream temperature regime. ASCE Specialty Conference, Utah State University, Utah, August 20–23, 1969. 35 p.

Yamaguchi, Y., Kahle, A.B., Pniel, M., Tsu, H., and Kawakami, T. (1998). Overview of Advanced Spaceborne Thermal Emission and Reflection Radiometer (ASTER). *IEEE Transactions on Geoscience and Remote Sensing*, 36 (4), 1062–1071.